NAVAL POSTGRADUATE SCHOOL

MONTEREY, CALIFORNIA

THESIS

DESIGN, TESTING, AND ANALYSIS OF SELF-TOSS HOPPING MANEUVERS OF ASTROBEE AT NPS AND NASA AMES RESEARCH CENTER

by

Conor P. Safbom

June 2020

Thesis Advisor: Marcello Romano
Co-Advisor: Stephen Kwok Choon, National Research Council

THIS PAGE INTENTIONALLY LEFT BLANK

REPORT DOCUMENTATION PAGE	*Form Approved OMB No. 0704-0188*

1. AGENCY USE ONLY *(Leave blank)*	**2. REPORT DATE** June 2020	**3. REPORT TYPE AND DATES COVERED** Master's thesis

4. TITLE AND SUBTITLE
DESIGN, TESTING, AND ANALYSIS OF SELF-TOSS HOPPING MANEUVERS OF ASTROBEE AT NPS AND NASA AMES RESEARCH CENTER

5. FUNDING NUMBERS

6. AUTHOR(S) Conor P. Safbom

7. PERFORMING ORGANIZATION NAME(S) AND ADDRESS(ES)
Naval Postgraduate School
Monterey, CA 93943-5000

8. PERFORMING ORGANIZATION REPORT NUMBER

9. SPONSORING / MONITORING AGENCY NAME(S) AND ADDRESS(ES)
N/A

10. SPONSORING / MONITORING AGENCY REPORT NUMBER

11. SUPPLEMENTARY NOTES The views expressed in this thesis are those of the author and do not reflect the official policy or position of the Department of Defense or the U.S. Government.

12a. DISTRIBUTION / AVAILABILITY STATEMENT
Approved for public release. Distribution is unlimited.

12b. DISTRIBUTION CODE
A

13. ABSTRACT (maximum 200 words)

Robotic hopping is a novel approach to microgravity mobility for a small spacecraft to use a robotic arm manipulator to toss a vehicle toward a destination. The Spacecraft Robotics Laboratory (SRL) at the Naval Postgraduate School (NPS) has demonstrated the viability of this mobility approach on its microgravity research testbed, POSEIDYN. SRL shall attempt this mobility approach with NASA's Astrobee free-flyer, a small robotic research platform designed to operate in microgravity, onboard the International Space Station. In preparation for this experimental campaign, self-toss maneuvers were tested at both NPS and at NASA Ames Research Center. These maneuvers were performed using Astrobee's existing perching arm, and a variety of initial and end angles were tested for both the distal and proximal joints of the arm. This thesis analyzed these results and presented the path ahead for SRL's research with Astrobee.

14. SUBJECT TERMS
Astrobee, ISS, robotics, space, NASA, astronautics, International Space Station, hopping maneuver, dynamics, multibody robotic system, autonomy, zero gravity, Python, Raspberry Pi, engineering, aerospace, modeling, calibration, free-flyer, Spacecraft Robotics Laboratory, SRL, POSEIDYN, NASA Ames

15. NUMBER OF PAGES
95

16. PRICE CODE

17. SECURITY CLASSIFICATION OF REPORT	**18. SECURITY CLASSIFICATION OF THIS PAGE**	**19. SECURITY CLASSIFICATION OF ABSTRACT**	**20. LIMITATION OF ABSTRACT**
Unclassified	Unclassified	Unclassified	UU

NSN 7540-01-280-5500

Standard Form 298 (Rev. 2-89)
Prescribed by ANSI Std. 239-18

THIS PAGE INTENTIONALLY LEFT BLANK

Approved for public release. Distribution is unlimited.

DESIGN, TESTING, AND ANALYSIS OF SELF-TOSS HOPPING MANEUVERS OF ASTROBEE AT NPS AND NASA AMES RESEARCH CENTER

Conor P. Safbom
Ensign, United States Navy
BS, U.S. Naval Academy, 2019

Submitted in partial fulfillment of the
requirements for the degree of

MASTER OF SCIENCE IN ASTRONAUTICAL ENGINEERING

from the

NAVAL POSTGRADUATE SCHOOL
June 2020

Approved by: Marcello Romano
Advisor

Stephen Kwok Choon
Co-Advisor

Garth V. Hobson
Chair, Department of Mechanical and Aerospace Engineering

THIS PAGE INTENTIONALLY LEFT BLANK

ABSTRACT

Robotic hopping is a novel approach to microgravity mobility for a small spacecraft to use a robotic arm manipulator to toss a vehicle toward a destination. The Spacecraft Robotics Laboratory (SRL) at the Naval Postgraduate School (NPS) has demonstrated the viability of this mobility approach on its microgravity research testbed, POSEIDYN. SRL shall attempt this mobility approach with NASA's Astrobee free-flyer, a small robotic research platform designed to operate in microgravity, onboard the International Space Station. In preparation for this experimental campaign, self-toss maneuvers were tested at both NPS and at NASA Ames Research Center. These maneuvers were performed using Astrobee's existing perching arm, and a variety of initial and end angles were tested for both the distal and proximal joints of the arm. This thesis analyzed these results and presented the path ahead for SRL's research with Astrobee.

THIS PAGE INTENTIONALLY LEFT BLANK

TABLE OF CONTENTS

LIST OF FIGURES

THIS PAGE INTENTIONALLY LEFT BLANK

LIST OF TABLES

THIS PAGE INTENTIONALLY LEFT BLANK

LIST OF ACRONYMS AND ABBREVIATIONS

APK	Android Package
ARC	Ames Research Center
CDH	Command and data handling
DOF	degrees-of-freedom
EVA	Extravehicular Activity
FSS	floating spacecraft simulator
GNC	Guidance, navigation, and control
HLP	High-Level Processor
IRG	Intelligent Robotics Group
ISAS	Institute of Space and Astronautical Science
ISS	International Space Station
IVA	Intravehicular Activity
JAXA	Japanese Aerospace Exploration Agency
LLP	Low-Level Processor
ManiSat	Manipulator Satellite
MGTF	Micro-Gravity Test Facility
MLP	Mid-Level Processor
NASA	National Aeronautics and Space Administration
NPS	Naval Postgraduate School
POSEIDYN	Proximity Operation of Spacecraft: Experimental hardware-In-the-loop DYNamic simulator
ROS	Robot Operating System
SPHERES	Synchronized Position Hold Engage Reorient Experimental Satellites
SRL	Spacecraft Robotics Laboratory
USOS	United States Orbital Segment

THIS PAGE INTENTIONALLY LEFT BLANK

ACKNOWLEDGMENTS

Completing a graduate program takes a village, and mine was full of the most supportive and encouraging people from the beginning. I would like to thank a few of the important individuals who have made this thesis possible.

I must first begin by thanking my thesis advisor, Dr. Marcello Romano. I had barely begun classes here at the Naval Postgraduate School when I received an email from him describing the exciting work that was being done in the Spacecraft Robotics Laboratory. From our first meeting, I knew this was the research I wanted to participate in.

Dr. Stephen Kwok Choon, my co-advisor, was instrumental to the completion of my thesis. I worked with him almost daily during my third and penultimate quarter here. I have learned so much from Dr. Kwok Choon about research and the will it takes to work through frustration, which there was plenty of this year. He is a brilliant person who has much to contribute to his field and to the education of future engineers.

The entire Astrobatics team, including LT Jonathan Chitwood, LT Daniel Watanabe, LT James Summerlin, and ENS Patrick Leary, have all been incredible companions and partners in this project. They have produced some impressive work over this past year. They are all incredibly intelligent people, and I know the project is in the best possible hands following my departure.

Finally, I want to thank my loving and encouraging parents, Dan and Terri. I had some tough days throughout my time at NPS, including a painful loss, but I weathered it all with the backing of my Mom and Dad. None of this would have been possible without your support, wisdom, and love throughout my entire academic career.

THIS PAGE INTENTIONALLY LEFT BLANK

I. INTRODUCTION

A. ROBOTIC HOPPING MANEUVER

A robotic hopping maneuver is defined as a propellant-less method of mobility for spacecraft. A robotic arm manipulator is used to provide the necessary force to traverse between two locations, similar to an astronaut pushing off one interior wall of the International Space Station and then grasping a destination handrail. A typical hopping maneuver consists of a push, free-flying coast, and a soft-landing, as shown in Figure 1 for a spacecraft traveling between two handrails.

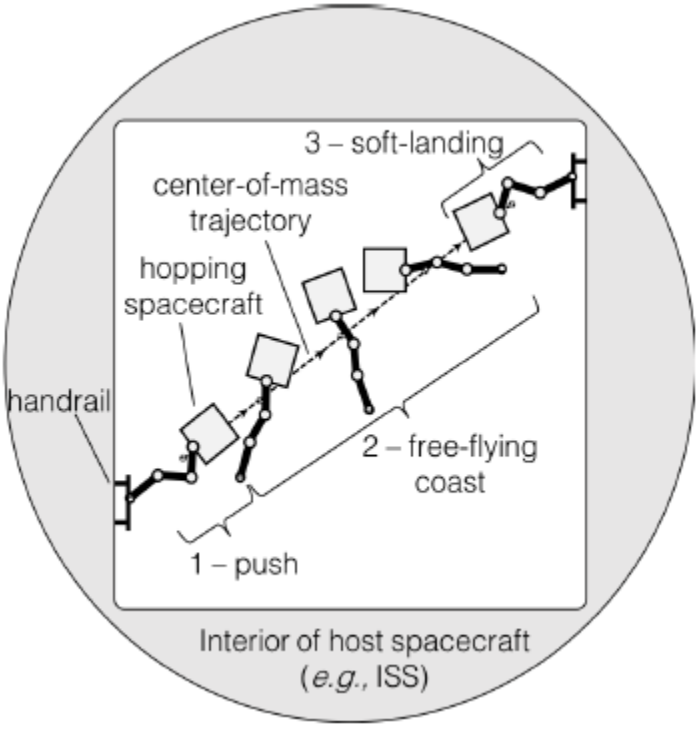

Figure 1. Schematic of robotic hopping maneuver. Source: [1].

This method is being developed to address the limitations of the two other mobility approaches currently used by robotic spacecraft: zero-g climbing and propulsive free-flying [2]. Zero-g climbing replicates how an astronaut would maneuver around the outside of the ISS during an Extravehicular Activity (EVA); instead of "hopping" between

handrails, the spacecraft always has constant contact with at least one handrail. There is no free-flying coast in this mobility approach, and therein lies the chief limitation of this maneuver: to reach a destination, a spacecraft must utilize the handrails within its physical reach, and it must have more than one robotic arm manipulator. NASA's Robonaut, a humanoid robot currently onboard the ISS, utilizes zero-g climbing to maneuver within the US Orbital Segment (USOS) [2].

Propulsive free-flying is the use of onboard propellant and thrusters to move from one location to another and has been used by spacecraft since the early days of spaceflight. The obvious limitation of this approach is that propellant is a finite resource and refueling spacecraft in orbit is not a trivial operation. Recharging a robotic spacecraft's batteries using solar panels, however, is a routine orbital operation, thus allowing the persistent use of a robotic arm manipulator for hopping maneuvers. Propulsive free-flying has a few advantages: the spacecraft is free to move within 3-dimensional space and is not limited to destinations that can be interfaced with by a robotic arm manipulator. Propulsive free-flyers can perform mid-course corrections that would be impossible through actuations of a robotic arm alone. In order to execute a soft-landing using a hopping maneuver, it may in fact be necessary to use a combination of external thrusters and internal momentum exchange devices to reduce both linear and angular velocities of the spacecraft. However, the use of thrusters would still be minimized because they did not have to provide the initial linear or angular velocities necessary for the maneuver.

B. ASTROBEE

Astrobee is a cuboid free-flying robot intended for Intravehicular Activity (IVA) experimentation onboard the International Space Station (ISS). The three primary functions of Astrobee are:

- Mobile sensing capabilities (e.g., air quality measurements or mobile cargo inventory)
- Mobile camera tasks (e.g., astronaut experiment recording)
- Provide zero gravity robotic research capabilities for governmental and academic entities [3]

1. Vehicle Description

Figure 2 shows two external views of the Astrobee free-flyer, including its main components.

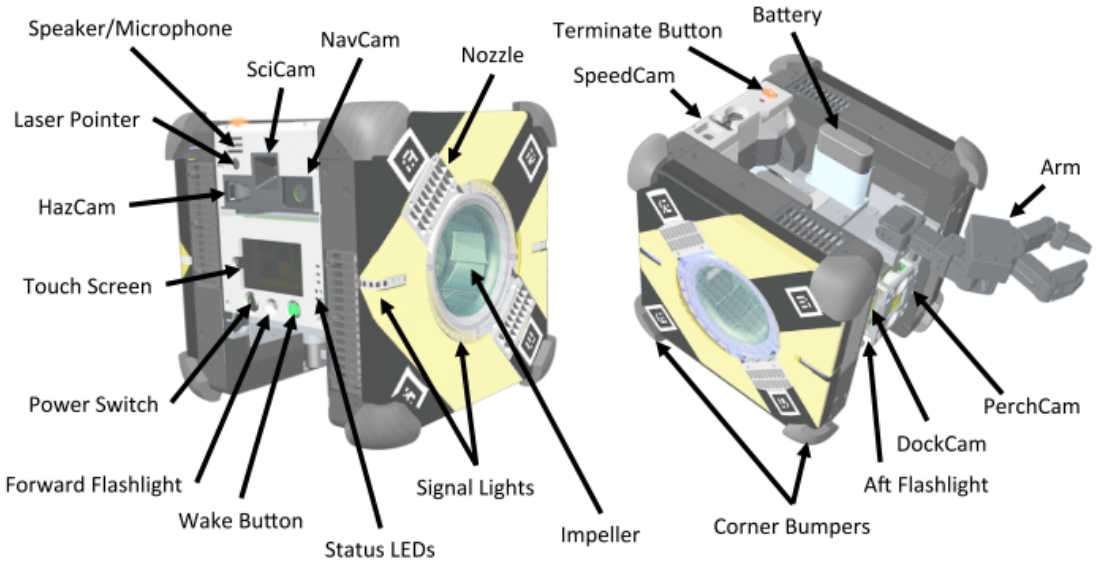

Figure 2. Diagram of Significant Astrobee components. Source: [4].

According to the Intelligent Robotics Group (IRG) at NASA Ames Research Center (ARC) [3], Astrobee is described by the following subsystems:

- Structure: The free-flyer is approximately 32 x 32 x 32-cm (1 ft^3) cube, with an exterior shell composed of Ultem and aluminum. The structure is designed to be lightweight but also capable of surviving impacts with the interior walls of the USOS.

- Propulsion: Two impellers on either side of Astrobee pressurize interior plenums that provide airflow to 12 exterior nozzles that are present on every single face of the free-flyer, resulting in six-degree-of-freedom holonomic control. There are two propulsion modules, one on each side of the vehicle.

- Power: Astrobee is powered by rechargeable lithium ion batteries, and the free-flyer is designed to autonomously return to its docking station when its power is low.

- Guidance, Navigation, and Control (GNC): Astrobee utilizes vision-based navigation in order to maneuver within the USOS. Visual landmarks will allow autonomous flight through the space station and serve as waypoints when directed by the crew or ground operators.

- Command and Data Handling (CDH): Onboard CDH is handled by a three-tier processing system consisting of: a Low-Level Processor (LLP), which provides closed-loop control between the Inertia Measurement Unit and the two propulsion modules and converts required body forces and torques to thrust commands; a Mid-Level Processor (MLP), which runs the perching arm and hosts the majority of the vehicle's flight software; and a High-Level Processor (HLP), where guest science software is hosted and the user interface is controlled.

- Avionics: Astrobee's avionics modules are housed on either side of the free-flyer along with both propulsion modules and are heavily reliant on the LLP and MLP.

- Communications: Primary communication with Astrobee is accomplished through the ISS's onboard Wi-Fi network. Data can be routed through the station's LAN network and NASA's Ku-Band system down to ground controllers.

- Docking Mechanism: Each docking station can berth and charge up to two free-flyers in addition to having charging ports for four additional battery packs that can be installed manually by the crew. Each free-flyer will be capable of autonomously returning to the docking port.

- Perching Arm: The free-flyer's robotic arm manipulator is stowable and can grasp handrails within the USOS (Figure 3), and will be further explored in the following section due to its heightened importance to NPS' research [3].

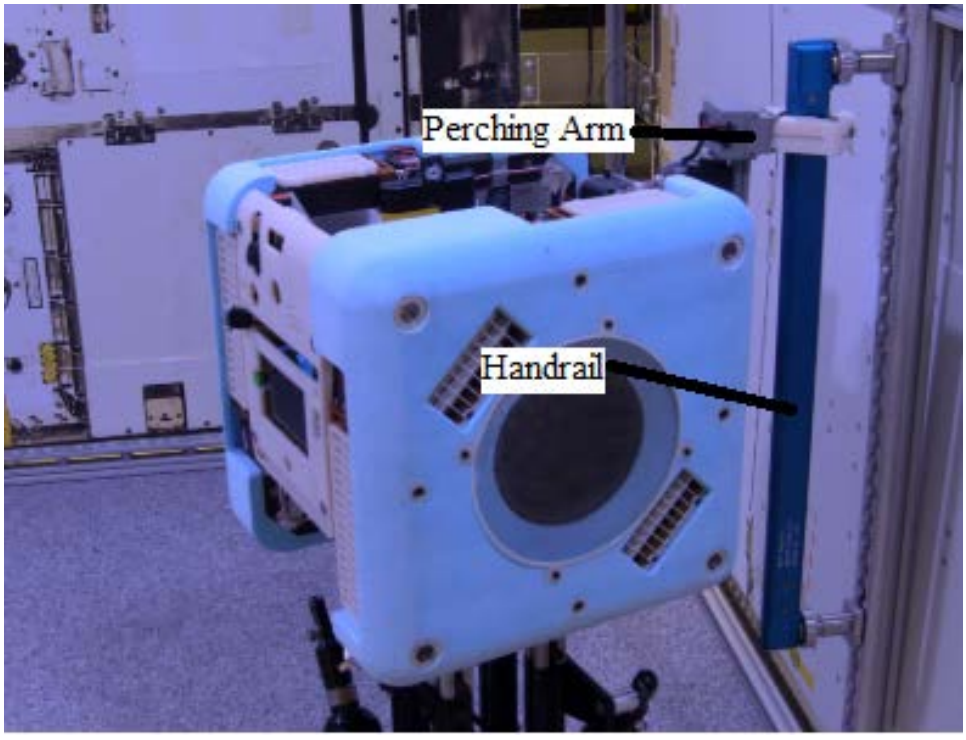

Figure 3. Demonstration of Astrobee perching capability. Adapted from [5].

2. Perching Arm

The most integral component of Astrobee to NPS' research is the 3-DOF compliant perching arm. The arm serves two purposes that it must balance: provide a platform for manipulation research, and fulfill the operational requirement to perch on ISS handrails in order to reduce the use of Astrobee's propulsion system [5].

The manipulator consists of a 2-DOF arm and a 1-DOF passively underactuated tendon-driven gripper, all of which is intended to be swappable should any guest scientist wish to test an advanced gripper or manipulator design. The tendon-driven gripper was chosen over options, such as electro-adhesion or gecko end-effectors, not only for its ability to grasp handrails, but also because the cluttered interior of the USOS is not an optimal environment for an end-effector that demands open flat spaces for perching.

The entire perching arm assembly is itself a separate payload that can be slid in and out of Astrobee's payload bay by astronauts with ease, and it is designed to be entirely contained within the protective envelope of the vehicle's outer shell when it is in its stowed position, as shown in Figure 4.

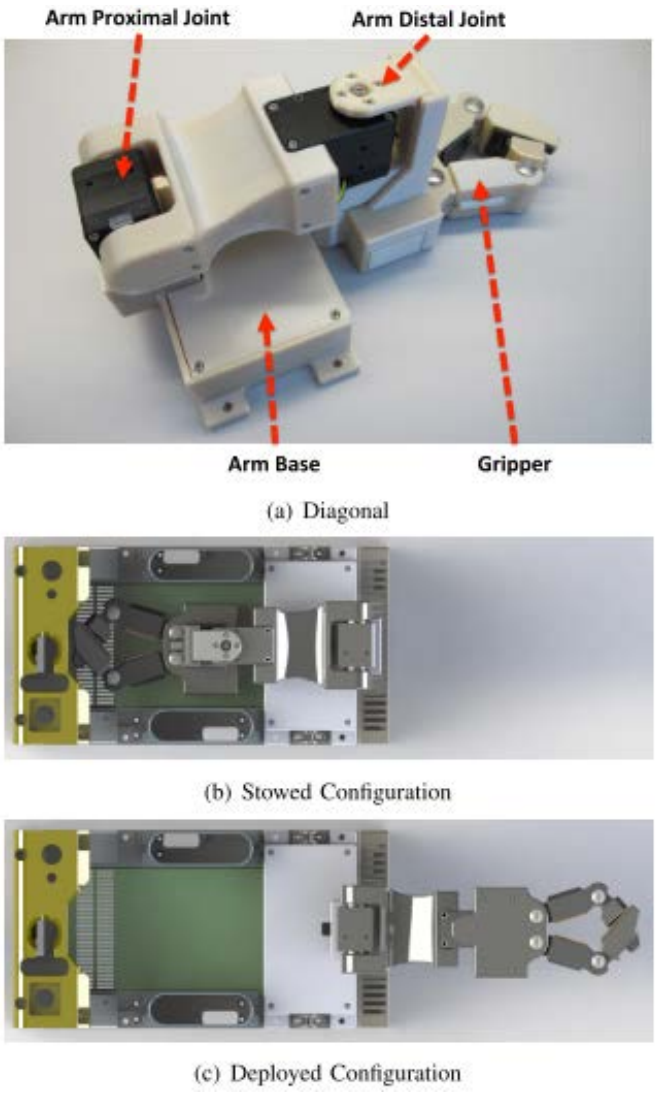

Figure 4. Astrobee perching arm. Source: [5].

NPS plans to make use of both the proximal and distal joints in its robotic hopping research, so an understanding of the physical limitations of each when perched on a handrail is important. Depending on the distance, planar hopping maneuvers from one handrail to another may require a motor joint to actuate through most of its physical range in order to produce the required linear and angular momentum to perform the maneuver with minimal thruster corrections. When Astrobee is perched on a handrail, it is designed to support pan-tilt maneuvers to allow the repositioning of the SciCam camera for experiment recording purposes. The ranges allowed for the pan-tilt capability are displayed in Figure 5.

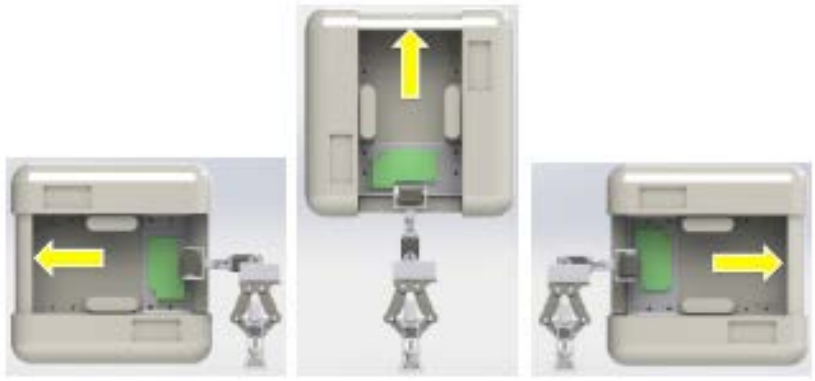

(a) Pan range of -90.0° to 90.0°

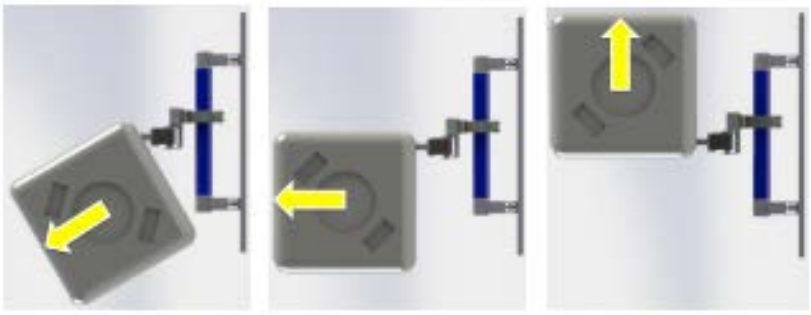

(b) Tilt range of -30.0° to 90.0°

Figure 5. Ranges for pan (distal joint) and tilt (proximal joint). Source: [5].

3. Guest Science Payload

Each of the three Astrobee free-flyers sent to the ISS will host a significant amount of guest research from a variety of governmental and academic institutions, including NPS. The IRG has identified a list of research themes that cover space technology research including motion control, advanced propulsion, robotic manipulation, robotic swarms and formation flight, satellite diagnostics, and astronaut-robot interactions [4]. Some institutions require the installation of new hardware to perform their research, and therefore the perching arm was designed to be easily modified or entirely removed from each free-flyer.

Each Astrobee has three payload bays available for guest science use, one of which is occupied when the perching arm is installed (see Figure 6). Guest payloads can be designed to interface with these bays by designing quick-release levers that can be captured

by the two clevises present in each bay, or by installing captive bolts into the pattern of four bolt-holes in each bay [4].

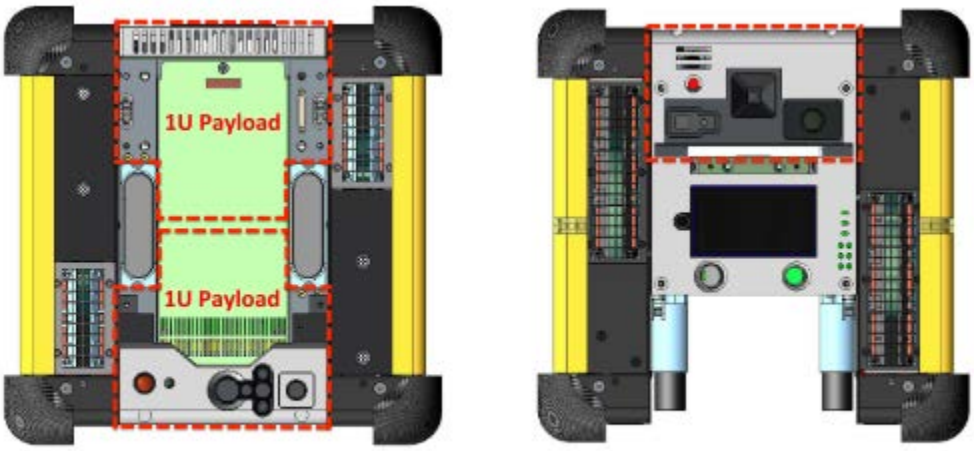

Figure 6. Astrobee payload bays. Source: [5].

Some guest science will not require any hardware modifications to the free-flyer but will instead rely on software that can be executed within the HLP of Astrobee's CDH architecture. The SRL will not be sending any hardware to the ISS as its research intends to demonstrate the viability of the robotic hopping maneuver using the existing perching arm. Depending on the length of Astrobee's mission onboard the ISS, it may be beneficial in the future for the SRL to design a robotic arm manipulator and gripper purpose-built for hopping maneuvers.

C. RESEARCH OBJECTIVES

Robotic hopping maneuvers have been studied extensively at NPS, and that work is detailed in Chapter III following a review of the laboratory facilities used during those experiments and the ones to be discussed later in this thesis. The overall objective of the new research detailed in this document was to independently verify the dynamic modeling developed for this maneuver, in addition to performing the experiments necessary to secure ISS crew time. Most importantly, robotic hopping maneuver experiments with Astrobee were carried out at NASA ARC for the first time, and a comparison between the results collected at both facilities will be presented.

D. THESIS OVERVIEW

This maneuver has been tested on the ground, and this thesis shall cover the work that has been done in the lead up to the ISS experimental campaign. Chapter II will describe the facilities used to test this maneuver. Chapter III will provide an overview of the state of the art in robotic hopping, with sections on both the general community and NPS research. Chapter IV will describe the hopping maneuver concept in more detail, to include the concept of operations, generalized equation of motions, software used to both simulate the maneuver and control Astrobee, and the hardware utilized at NPS and Ames to test the maneuver. Chapter V will cover the entire experimental campaign that has been completed to date, in addition to addressing how the project will continue. Chapter VI provides the experimental results from experiments performed at both NPS and NASA Ames Research Center. Finally, Chapter VII provides concluding remarks and an overview for the project's future.

II. GROUND TESTING FACILITIES

In preparation for experimentation on board the ISS, a long campaign of ground testing must be completed at both NPS and NASA ARC. Both locations feature large air-bearing granite testbeds that can be used to test a notional robotic hopping maneuver in a high-fidelity, dynamically representative environment. After a brief introduction to microgravity research and air-bearing testbed technology, this chapter shall describe both facilities in detail.

It is impossible to replicate the microgravity environment present on the ISS or in space, except for parabolic flights or drop towers. However, these methods have several practical limitations, the most notable of which is time. Aircraft of the type used in microgravity experimentation can only freefall for about 20s before leveling off, and drop towers can only be built tall enough for experiments lasting between 5-10s (see Figure 7-Figure 8) [6].

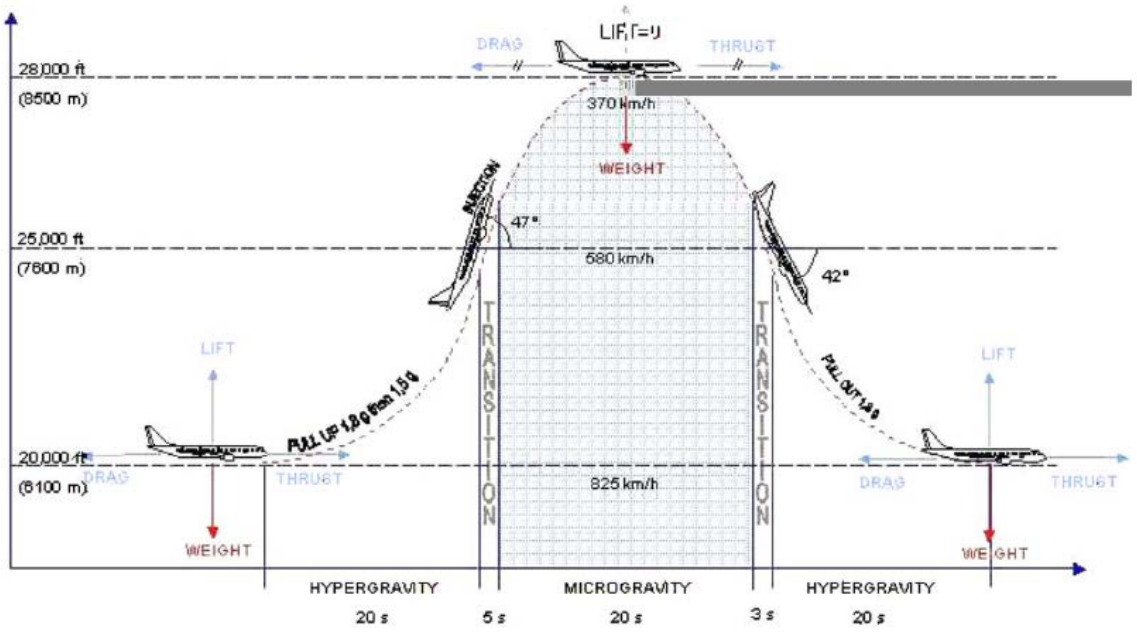

Figure 7. Parabolic flight profile of Airbus A300 'Zero-G,' used for microgravity research by the European Space Agency. Source: [7].

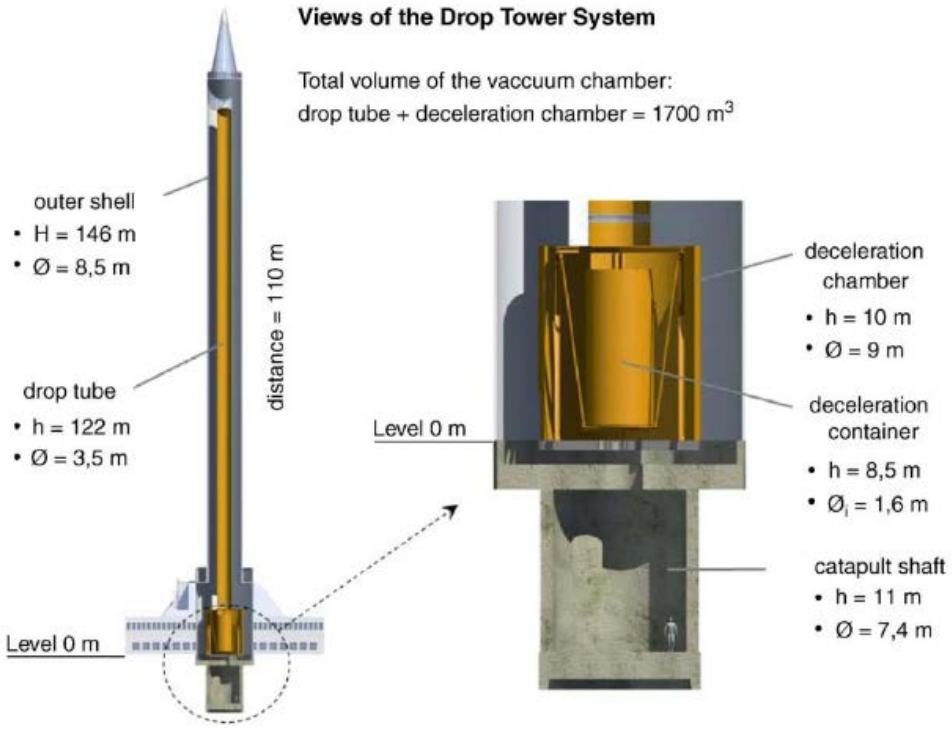

Figure 8. Schematic of catapult-assisted Drop Tower Bremen. Source: [8].

With these limitations in mind, researchers have developed several creative ways to approximate the frictionless environment present in space for longer durations, including using planar air-bearing microgravity simulators. These testbeds typically feature a large, flat planar surface made of an ultra-smooth material such as epoxy or in most cases, granite. The system to be tested is mounted on air-bearings that provide a thin, uniform film of pressurized gas (usually CO_2, despite the name) that results in a practically negligible friction coefficient, which in some systems is as low as 10^{-5}.

The major limitation of planar air-bearing microgravity simulators is their inability to simulate more than 3-DOF (two translational and one rotational), with the exception of a few specialized systems that introduce spherical air bearings to add more rotational DOF and complex counterweight systems to allow motion perpendicular to the testbed. While simulating 6-DOF could certainly be beneficial for Astrobee, all maneuvers using the perching arm are designed to be planar, so a 3-DOF system will provide adequate fidelity for experimentation.

A. NPS POSEIDYN

The Proximity Operation of Spacecraft: Experimental hardware-In-the-loop DYNamic simulator (POSEIDYN) testbed is NPS' primary asset in the development of the robotic hopping maneuver, in addition to several other projects in the field of autonomous rendezvous and proximity operations (RPO). The testbed is comprised of three primary elements: a 4 x 4 m granite monolith, floating spacecraft simulators (FSSs), and a motion camera-based metrology system (see Figure 9) [9].

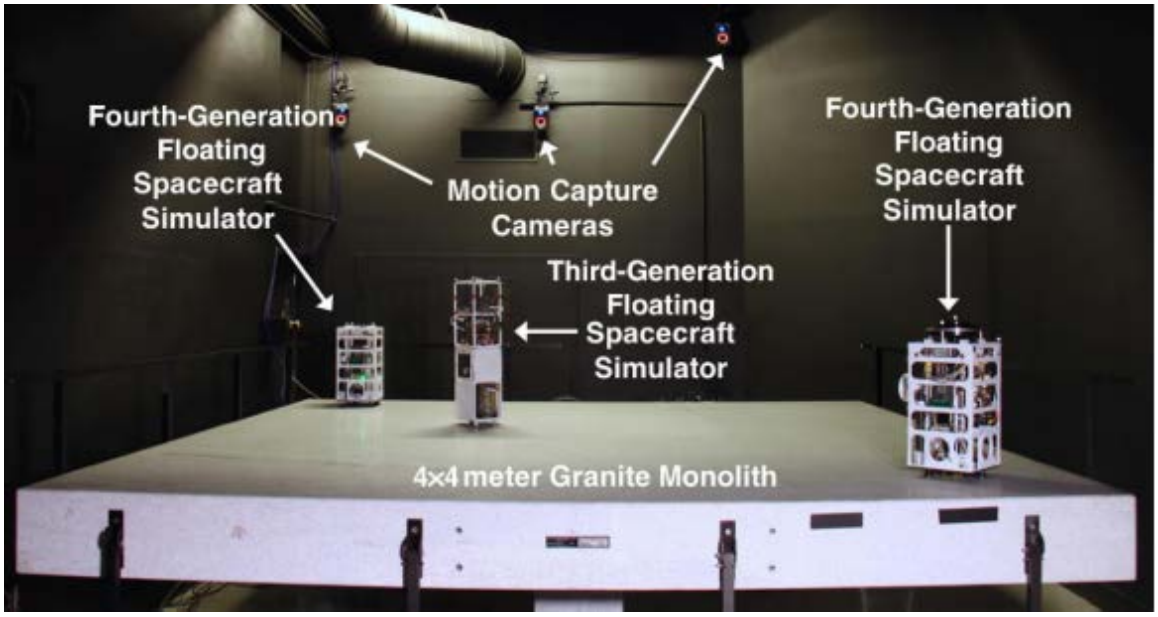

Figure 9. POSEIDYN. Source: [9]

1. Granite Monolith

The most visible component of POSEIDYN is the 4 x 4 m granite monolith located adjacent to the main room of the SRL in the lower level of Halligan Hall. The entire monolith has a mass of 15 metric tons and is suspended by three adjustable pedestals, intended for correcting planar accuracy. As of its most recent measurement, the monolith has a planar accuracy of ± 0.0127 mm and a level accuracy of 0.01 deg. This level accuracy and the monolith's precisely-ground granite surface allows for almost frictionless motion across the testbed when combined with the FSSs.

The size of the granite monolith limits the use of POSEIDYN to short-duration and close proximity maneuvers because there is no way to replicate orbital mechanics on such a constrained workspace. However, maneuvers involving Astrobee will be between either adjacent or parallel USOS walls, and the space available on the table is sufficient for modelling those distances.

2. Floating Spacecraft Simulators

The FSSs are NPS-developed mobile research platforms meant for small spacecraft operations research. Over the course of a decade, four generations of FSSs have been developed (see Figure 10). The 4th generation FSS remains in use by the SRL and is by far the most capable research platform in the series. It features three air-bearings that provide a consistent and equal amount of compressed air from an onboard 1.87 Liter tank held at $2.068e^7$ Pa (3000 psi). The air-bearings can produce a 5 μm air film between the FSS and the granite surface, resulting in negligible surface friction effects on FSS motion. This compressed air is easily refillable using a scuba-diving-type air compressor, conveniently collocated in a utility room adjacent to POSEIDYN.

Figure 10. Evolution of the Floating Spacecraft Simulator (FSS). Source: [9].

3. Vicon Metrology System

The motion-capture system of POSEIDYN was developed by Vicon and consists of ten cameras evenly placed at locations above the granite monolith. Passive markers are placed on every visible surface of FSSs used during experimentation, and the Vicon system is able to track those marker positions and thus the positions of the marked FSSs at a rate of up to 100 Hz and with an accuracy of less than 1 millimeter. Location data determined by the Vicon system is not only used for experimental analysis, but also most importantly for FSS navigation. Each FSS combines onboard sensor data and actuator states with the Vicon data via a discrete Kalman filter in order to generate accurate state estimates that can be read into the guidance and control subsystems (see Figure 11) [9].

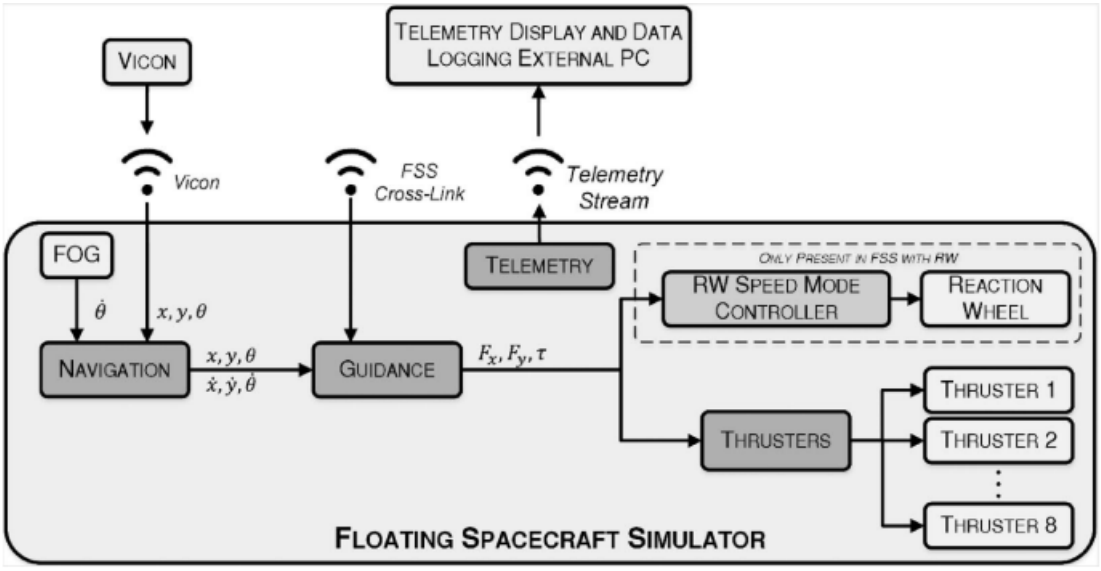

Figure 11. FSS Software Architecture. Source: [9].

B. NASA AMES RESEARCH CENTER FACILITIES

Most guest science payloads, whether they are alterations to the HLP or physical additions to Astrobee, require some testing to be completed at NASA ARC before experimentation can be performed onboard the ISS [4]. The IRG runs two facilities for this purpose: the Granite Lab and the Micro-Gravity Test Facility (MGTF). Both were previously used by the Synchronized Position Hold Engage Reorient Experimental Satellites (SPHERES) series of robotic free-flyers, which was a highly successful nano-satellite experiment that advanced research in the fields of formation flight, proximity operations, and autonomous docking (see Figure 12) [10].

Figure 12. Astronaut Scott Kelly interacting with SPHERES free-flyers. Source: [10].

1. Granite Lab

The Granite Lab is very similar to POSEIDYN; as the name implies, the facility features a 2 x 2 m granite monolith similar in horizontality and planarity to the NPS testbed. However, unlike POSEIDYN, which is used to replicate a variety of space-based scenarios and environments, the Granite Lab is meant strictly to simulate the interior of the USOS, and more specifically, the ISS node where Astrobee's docking station is located (see Figure 13). Another major difference is that localization and navigation are performed entirely onboard the test unit in the Granite Lab, as opposed to relying on a motion-camera system and DKF. Astrobee uses its own sensors and navigational cameras to detect landmarks to complete maneuvers. This setup is meant to replicate the conditions Astrobee will experience onboard the ISS. A Wi-Fi connection with a collocated ground station computer allows for real-time tracking of Astrobee's position, in addition to what it is "seeing" with its sensors and cameras. Telemetry can be downloaded from each test unit following use.

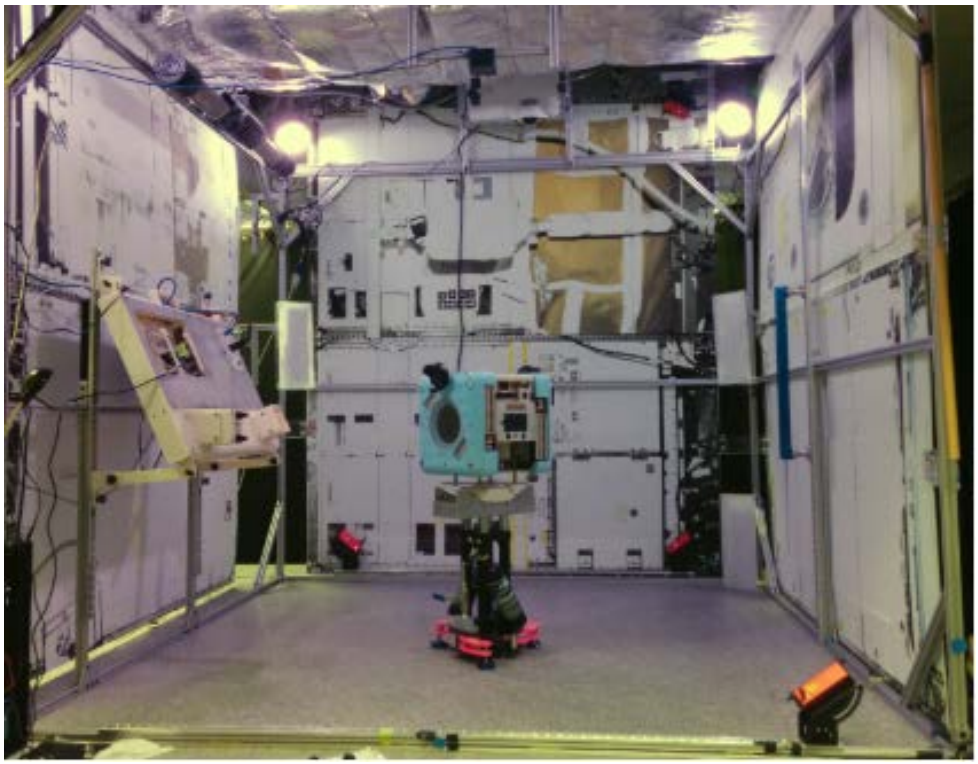

Figure 13. Granite Lab with 3-DOF Astrobee motion simulator. Source: [4].

2. Micro-Gravity Test Facility

The MGTF consists of a 6-DOF motion simulator situated in a larger simulated ISS module. In this facility, an Astrobee is suspended from the ceiling by an active gimbal system (see Figure 14-Figure 15). This active gimbal system can provide Astrobee 360 degrees in the yaw axis, 126 degrees in the roll axis, and 180 degrees in the pitch axis [4], [10]. The ultimate goal of the MGTF is to test perching and docking in 6-DOF, and in particular to test misaligned approaches that cannot be simulated in the Granite Lab. The major difference between the complementary labs is that the MGTF approximates the physics Astrobee would experience without actually using the onboard thrusters, whereas the Granite Lab allows researchers to test maneuvers while demonstrating the real dynamics [10].

Figure 14. The Micro-Gravity Test Facility. Source: [4].

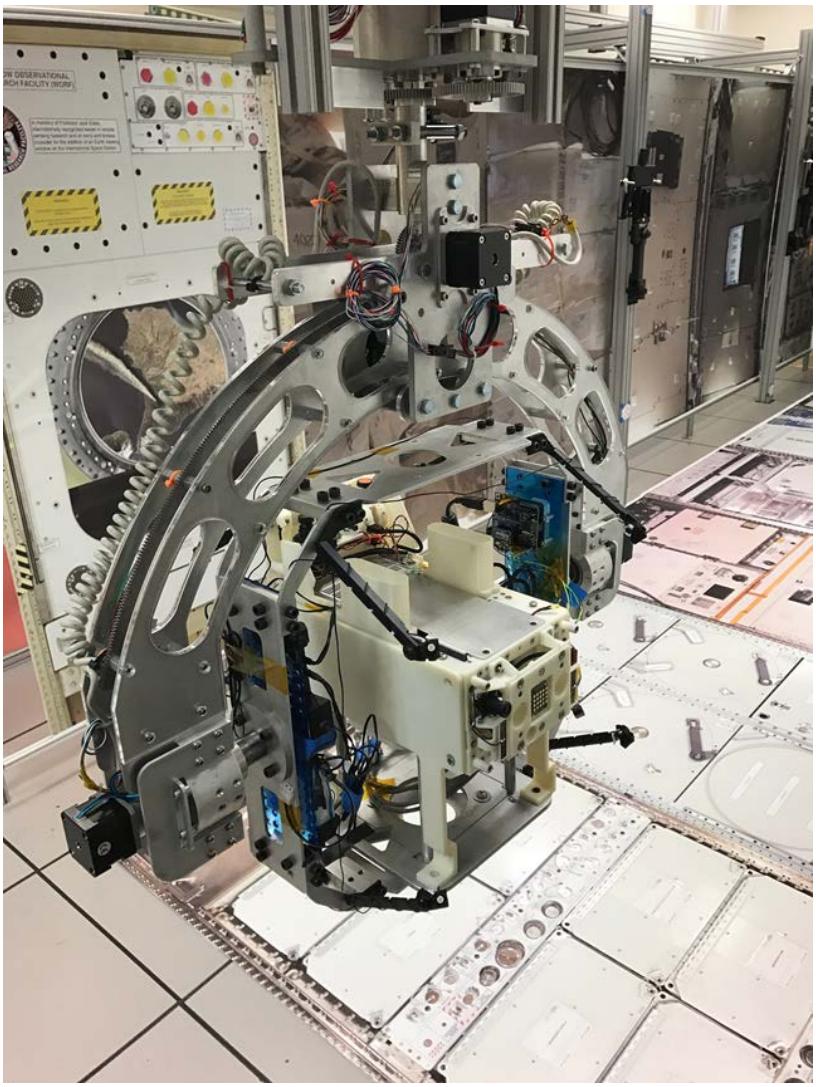

Figure 15. MGTF's active gimbal system and motion simulator. Source: [10].

THIS PAGE INTENTIONALLY LEFT BLANK

III. STATE OF THE ART

A. COMMUNITY RESEARCH

Space-based robotic hopping maneuvers have been explored with varying degrees of success by the wider robotics and astronautics communities since at least 1959. Much of the research in this field has been into propulsive hopping, such as the 2.4 m hop completed by the Surveyor 6 on the surface of the moon in 1967 [1]. This approach could allow lunar and planetary rovers the ability to explore large swathes of extraterrestrial surfaces without concern for the effects of rough terrain. However, propulsive hopping presents mission planners the same issue that propulsive free-flying does: propellant is finite. Propulsive hopping is certainly more effective in high-gravity environments, such as terrestrial applications or the surface of Mars; the impulse required to hop between locations exceeds what is currently possible with robotic arm manipulators. However, in micro-gravity environments such as the surface of an asteroid or inside the ISS, robotic hopping maneuvers could prove to be more effective, especially if the spacecraft can be continuously powered through the use of solar panels or recharged at a docking station.

A novel approach to robotic hopping was developed for Hayabusa2, a Japanese Aerospace Exploration Agency (JAXA) and Institute of Space and Astronautical Science (ISAS) mission to the C-type asteroid Ryugu that launched in 2014 and successfully arrived in mid-2018 [11], [12]. Onboard this spacecraft were twin rovers collectively named MINERVA-II. These rovers were deployed to the surface of Ryugu and represent the first successful deployment of robotic hopping maneuvers in space exploration and also resulted in the first image ever taken from the surface of an asteroid (see Figure 16). The two rovers demonstrated what their developers called “ciliary micro-hopping locomotion” [11]. Instead of a robotic arm manipulator, MINERVA-II utilized elastic cilia that provided the necessary impulse for each hop with the use of an attached eccentric motor (see Figure 17).

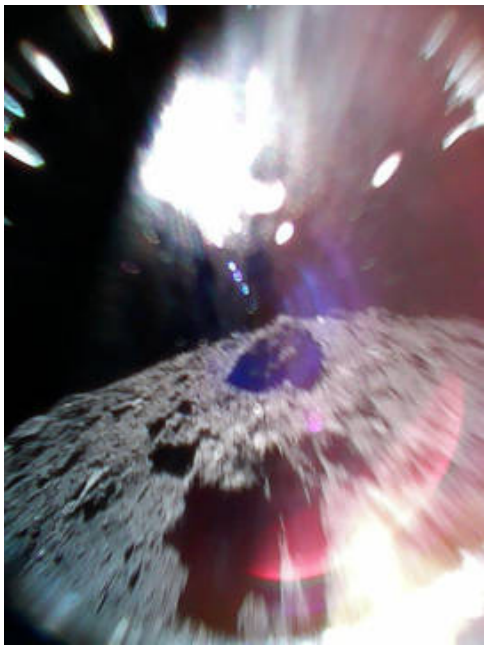

Figure 16. First image from surface of an asteroid, taken by MINERVA-II. Source: [12].

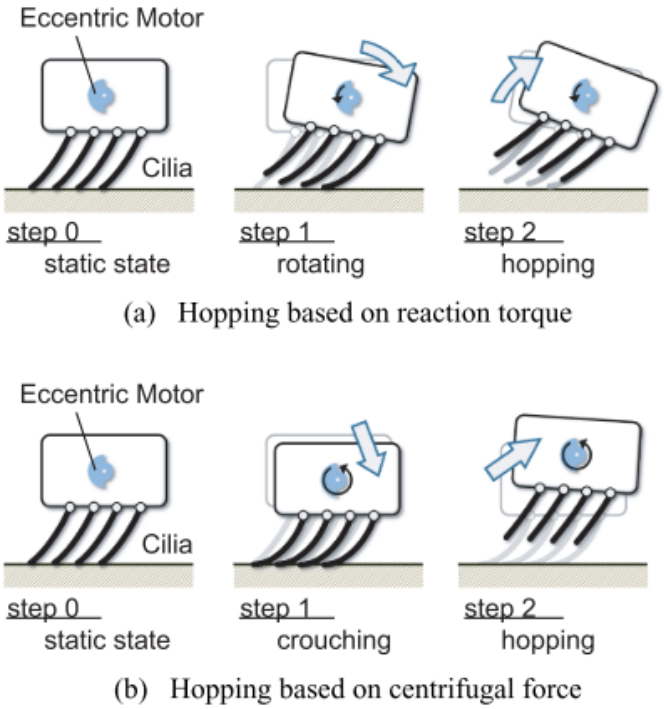

Figure 17. Ciliary micro-hopping locomotion approach to rover mobility. Source: [11].

B. NPS RESEARCH

1. Manipulator Satellite

The robotic hopping maneuver has been studied extensively at NPS in the Spacecraft Robotics Laboratory (SRL). Little research had been done on this mobility approach before NPS student Andrew Bradstreet's work on the Manipulator Satellite (ManiSat). ManiSat was a technology demonstration developed by NPS to investigate the effectiveness of a robotic hopping maneuver on a granite test-bed, the details of which will be expanded on in Chapter II [13]. ManiSat was composed of an NPS-developed Floating Spacecraft Simulator (FSS), two robotic arm manipulators with three degrees of freedom (DOF), and two grippers acquired and then 3D-printed from the open-source Yale OpenHand Project. The full system is displayed in Figure 18.

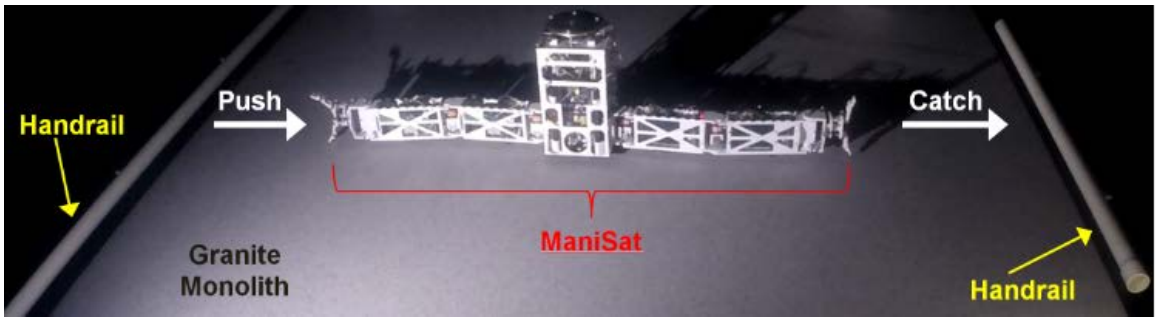

Figure 18. NPS ManiSat flying across Granite Table [13]

The success of these early experiments drove the SRL's decision to pursue further research into propellantless maneuvering of robotic spacecraft. One important detail to note is the presence of a "push" and "catch" arm, allowing for a simple hopping maneuver with minimal reaction wheel or thruster correction. A notional Astrobee hopping maneuver using a single 3-DOF perching arm will not benefit from the same simplicity.

2. Initial Astrobee Research

Following ManiSat, NPS began work on developing a propellantless maneuver for NASA's Astrobee free-flyer. Master's thesis student Katrina Alsup assisted in the development of the equations of motion that describe a robotic hopping maneuver

performed using Astrobee, in addition to running several simulations of so-called “soft” and “hard” landing hopping maneuvers [2]. A soft landing involves a robotic spacecraft reducing the relative velocity between its end effector and its destination handrail to almost zero. A hard landing, as the name suggests, simply does not have this requirement. The first analysis performed by Alsup was a study of the linear velocity envelope of Astrobee using both its proximal and distal joints. She found that robotic hopping maneuvers could achieve any direction and that they would not exceed the maximum joint velocities or the maximum safe velocity for operation inside the ISS (see Figure 19).

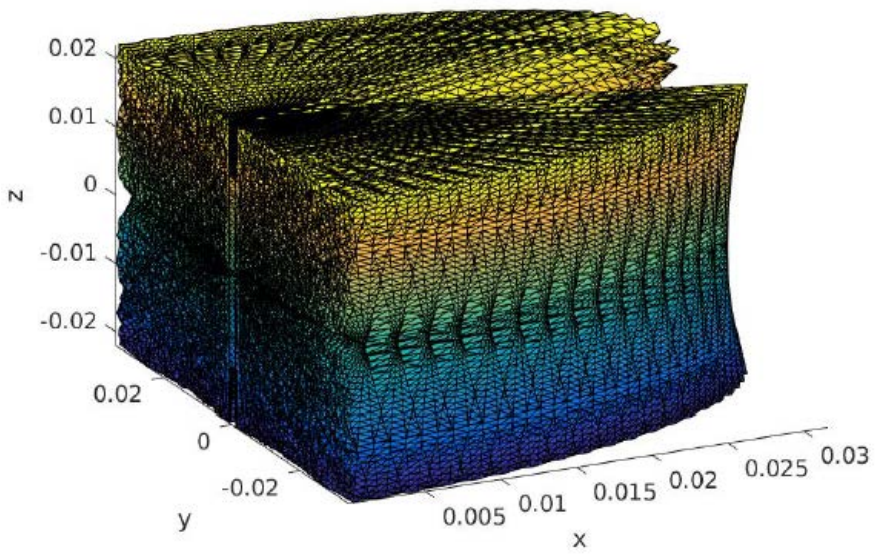

Figure 19. Linear velocity envelope for Astrobee (m/s). Source: [2].

Alsup’s follow-on research resulted in a full simulation of Astrobee’s motion during both soft and hard landing maneuvers. During a soft-landing maneuver, Astrobee actuates its proximal joint until it reaches its release angle, at which point the gripper releases the handrail and the joint holds the perching arm in place while Astrobee enters its coast phase. In order to achieve a soft landing, the proximal joint is again actuated moments before reaching the handrail in order to counteract the angular velocity of the vehicle. At this point, Astrobee will catch the destination handrail (see Figure 20). In a hard landing maneuver, the sequence is much the same, except there is no attempt to reduce the vehicle’s

angular velocity, choosing instead to arrest this motion through contact dynamics between the gripper and the destination handrail (see Figure 21). In both figures, the initial handrails are on the top right and the destination handrails are on the bottom left.

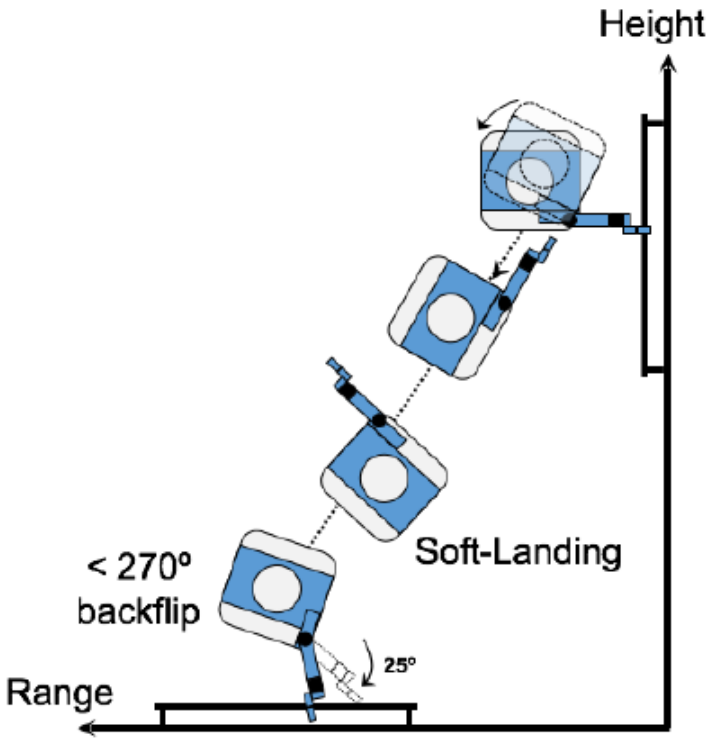

Figure 20. Astrobee soft landing schematic. Source: [2].

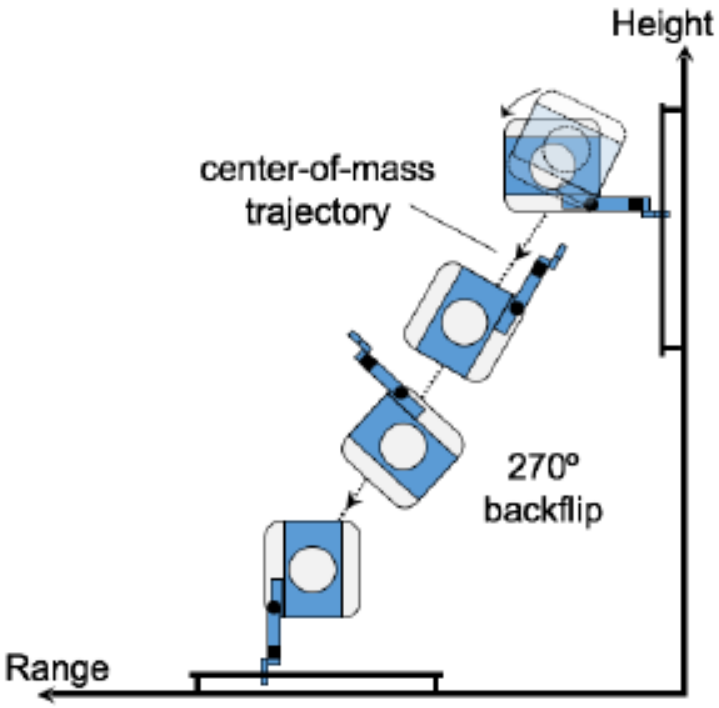

Figure 21. Astrobee hard landing schematic. Source: [2].

In both cases, the robotic hopping maneuver was determined to be technically feasible. However, Alsup also concluded that a true soft landing, with relative velocity between the gripper and destination handrail at 0 m/s, is not possible with the perching arm because of its limited DOF. It cannot both arrest angular velocity and negate linear velocity. Alsup recommended that a future manipulator with more DOF could achieve a true soft landing.

Master's thesis student Justin Komma assisted in the assembly and testing of a functional replica of Astrobee's robotic arm manipulator [14]. A CAD model of the perching arm was acquired from NASA, and the replica was assembled to be as dynamically similar to the real arm as possible. This replica arm was integrated with an FSS similar to ManiSat, and the main focus of Komma's experimentation was to answer the question of whether or not the existing perching arm could execute a "clean" hopping maneuver, "clean" meaning a maneuver with a minimal gripper slip angle (see 0). The slip angle is defined as the angle that the gripper rotates through before releasing the handrail.

An unpredictable slip angle could theoretically make reliably accurate hopping maneuvers virtually impossible, but Komma found that slip angles were repeatable and varied with the angular ranges that each maneuver rotated through before releasing the handrail. The maximum slip observed was 13.1 degrees during a 60-degree maneuver from -80 degrees to -20 degrees. Both Alsup and Komma concluded from simulation and physical testing that Astrobee's perching arm could feasibly demonstrate a robotic hopping maneuver onboard the ISS [2], [14].

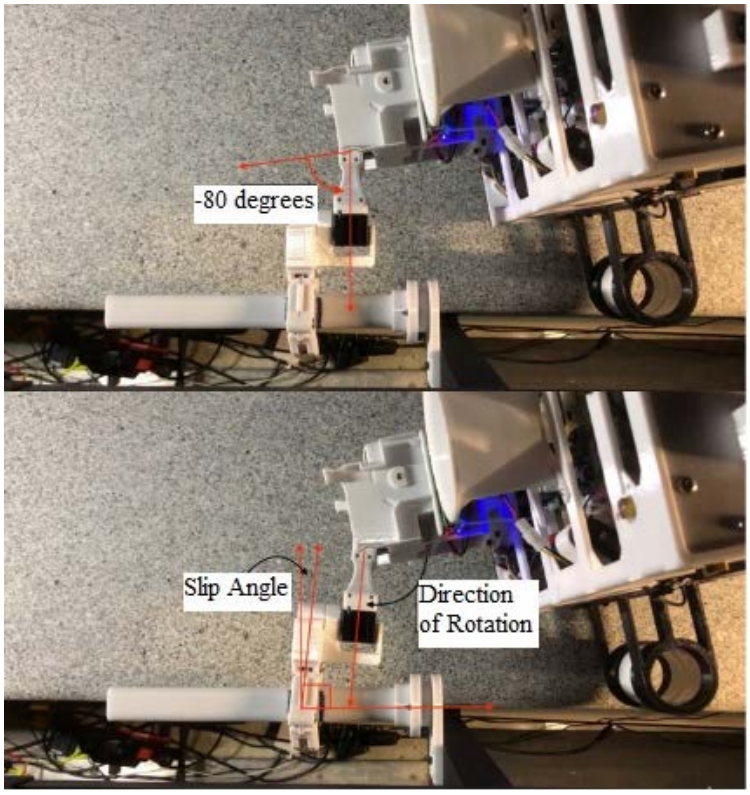

Figure 22. NPS Gripper slip angle demonstration. Source: [14]|

THIS PAGE INTENTIONALLY LEFT BLANK

IV. MANEUVER EXPERIMENTAL CAMPAIGN

Following the graduation of Justin Komma and Katrina Alsup, new experimental goals were set for the Spacecraft Robotics Laboratory, and more specifically the Astrobatics working group, which is dedicated to Astrobee hopping maneuver research. The first of these experimental goals was to not only replicate Komma's experiments but to do so using Astrobee's software. The perching arm used in both Komma's experimentation and the most recent round of testing was controlled by a Raspberry Pi 3, which is capable of understanding multiple programming languages. Due to developer recommendations, the software for the self-toss maneuvers tested in Komma's research was developed in Python. This software was never intended to be used as flight software; it was meant to prove that a hopping maneuver could be performed using a dynamically and mechanically accurate Astrobee perching arm. The challenge for SRL after this was proven was to develop software that could be utilized in Astrobee's guest science APK within the HLP.

The progression of ground experiments since this shift and going forward will follow a logical sequence of demonstrations of increasing complexity (see Table 1). Each row in this sequence corresponds to a specific demonstration to be performed onboard the ISS. The first experiment, S1, is a self-toss from a handrail through the USOS workspace. S2 will introduce stabilization by actuating the arm and minimal thruster use to zero out the vehicle's angular and linear velocities. S3 represents a full demonstration of a robotic hopping maneuver, whereby an Astrobee flight unity, referred to as AB1, will perform a self-toss and stabilization before gently perching on a destination handrail. S4 and S5 are intended to test a proposed Astrobee "handshake" maneuver, with two flight units using their grippers to grasp one another mid-flight.

Table 1. Astrobee Experimental Sequence. Source: [15].

	Vehicle	Maneuver
S1	AB1	• Self-Toss from Rail
S2	AB1	• Self-Toss from Rail • Stabilization
S3	AB1	• Self-Toss from Rail • Stabilization • Perching
S4	AB1	• IC: Grasping AB2 in mid-air • Self-Toss from AB2
	AB2	• Passively Logging Data
S5	AB1	• IC: Grasping AB2 in mid-air • Estimate Mass/Inertia of AB2
	AB2	• Passively Logging Data

Before any single demonstration in the experimental sequence can be conducted onboard the ISS, it is desired that each be tested on the ground at both NPS and at NASA ARC. However, waiting for crew time to conduct any of the demonstrations does not preclude SRL from beginning work on the next item in the sequence. Crew time is a valuable and highly in-demand resource, and SRL cannot always expect to receive timely results from on-orbit experimentation. The time period between each ISS demonstration gives SRL time to perform each maneuver on POSEIDYN and NASA ARC's Granite lab test bed, both described in detail in Chapter II.

The normal progression for ground experiments is to first attempt a range of maneuvers using a 4th Generation FSS and replica perching arm before taking the software to NASA ARC and implementing onboard their full-scale Astrobee test unit. Currently, SRL is preparing for S1, and this chapter will describe the experiments it has conducted thus far in order to be flight-ready for the first robotic self-toss demonstration in space.

A. NPS EXPERIMENTS

Experiments conducted on the POSEIDYN testbed were split into two groups: maneuvers using the proximal joint and the distal joint. The purpose of these first several tests was to determine if there was an optimal joint and an optimal range of initial and ending joint angles for the hopping maneuver. For both joints, three initial angles and five

final angles were chosen from the angular ranges depicted in Figure 23. These two variables represented the control variables for each experiment and defined how each experiment was identified for analysis and convenience. In order to determine repeatability, each experiment was run at least three times, sometimes more if more data sets for a particular angular range were desired.

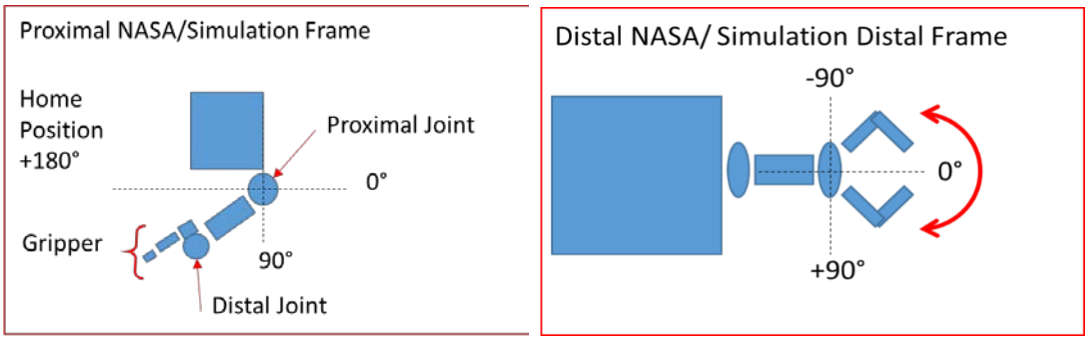

Figure 23. Frame for proximal and distal joints of perching arm.

1. Procedure

Before testing, the FSS' onboard air tank is pressurized to 20,684 kPa (3000 psi) and its two large battery packs are fully charged. Once the FSS is prepared, it is switched on via a small button to the left of the perching arm. To pressurize the air bearings, a valve is opened at the top of the air tank, which allows the compressed air to flow to the air bearing system, and then a switch above the power button is flipped to activate all three air bearings. The FSS must be moved to the handrail on the other side of the testbed while its air bearings are active, and those air bearings should then be switched off until the remaining preparations are complete to conserve air. Spherical tracking markers are placed on the main FSS body and on the links and joints of the perching arm. The markers on the FSS must be aligned with the vehicle's center of mass, +x axis, and placed in at least 2 other areas.

The next step is to initialize the motion tracking system via the Vicon computer next to the granite monolith. For this setup, two "vehicles" are tracked: the FSS base and the perching arm assembly. Both objects must be created within the Vicon software before

the experiment can be conducted. The MATLAB script 'Vicon_capture.m' is then run to verify that the motion tracking system is active. The ten Vicon cameras located around the testbed should all be green, as well.

MATLAB is used to collect and record telemetry from the FSS and the perching arm assembly, which are labeled 'vehicle1' and 'vehicle2' for each run, respectively. A Simulink model can be opened by the ground station operator to visualize the telemetry. The Vicon system records the FSS' movement with submillimeter level accuracy, and the corresponding MATLAB data files produced after each run provide position values for all three axes in addition to theta values as defined by the user-set +x axis.

One laboratory assistant manages the ground station while another monitors the FSS and positions the perching arm. From the ground station, a command is sent to the perching arm module Raspberry Pi to execute a particular maneuver. The perching arm starts in the stowed position and then moves to the initial joint angle of the commanded maneuver with its gripper open. The other lab assistant activates the air bearings and moves the entire vehicle such that when the gripper is closed, its fingers will encircle the handrail. For consistency, a location on the handrail has been marked so that the gripper starts from the same place during every run. Once the FSS' motion has been stabilized, the maneuver can be commanded, and the data recorded. The lab assistant monitoring must constantly check the air tank's pressure; it is recommended that the air tank be re-pressurized if the gauge dips below 1500 psi. The air-bearings begin dragging if the pressure drops too low, but the effects on FSS motion can be imperceptible to the human eye. The effects to the recorded data, however, can be substantial.

Safe shutdown of the entire POSEIDYN system begins with commanding the Raspberry Pi to shut off and then exiting the command terminal of the ground station. All stored data must then be organized into a file directory identified by the joint tested and the date of experimentation. The Vicon system is then shut down by first clicking "Ok: on the "Stop Capture" prompt, and then closing both the MATLAB motion capture streaming script and the Vicon software. Finally, the Vicon control box is powered down and the shutdown procedure is complete.

2. Proximal Joint Maneuvers

Testing proximal self-toss maneuvers required no hardware modifications to the replica perching arm, FSS, or the 3D-printed replica ISS handrail as originally assembled by Justin Komma during his experimentation.

Table 2 shows the initial experiments that have been conducted with POSEIDYN. Every maneuver marked in yellow is a testable range for the perching arm. Some maneuvers, marked with red stripes, are outside of the operational boundaries and were not tested. Maneuvers marked in red are not practical because they do not result in the actuation of the arm.

Table 2. NPS proximal joint experiments

Initial Proximal Angle (°)	Final Proximal Goal (°)						
	0	15	30	45	60	75	90
30	Outside Scope	Valid	Not applicable	Valid	Valid	Valid	Outside Scope
45	Outside Scope	Valid	Valid	Not applicable	Valid	Valid	Outside Scope
60	Outside Scope	Valid	Valid	Valid	Not applicable	Valid	Outside Scope

Legend	
	Valid
	Not applicable
	Outside Scope

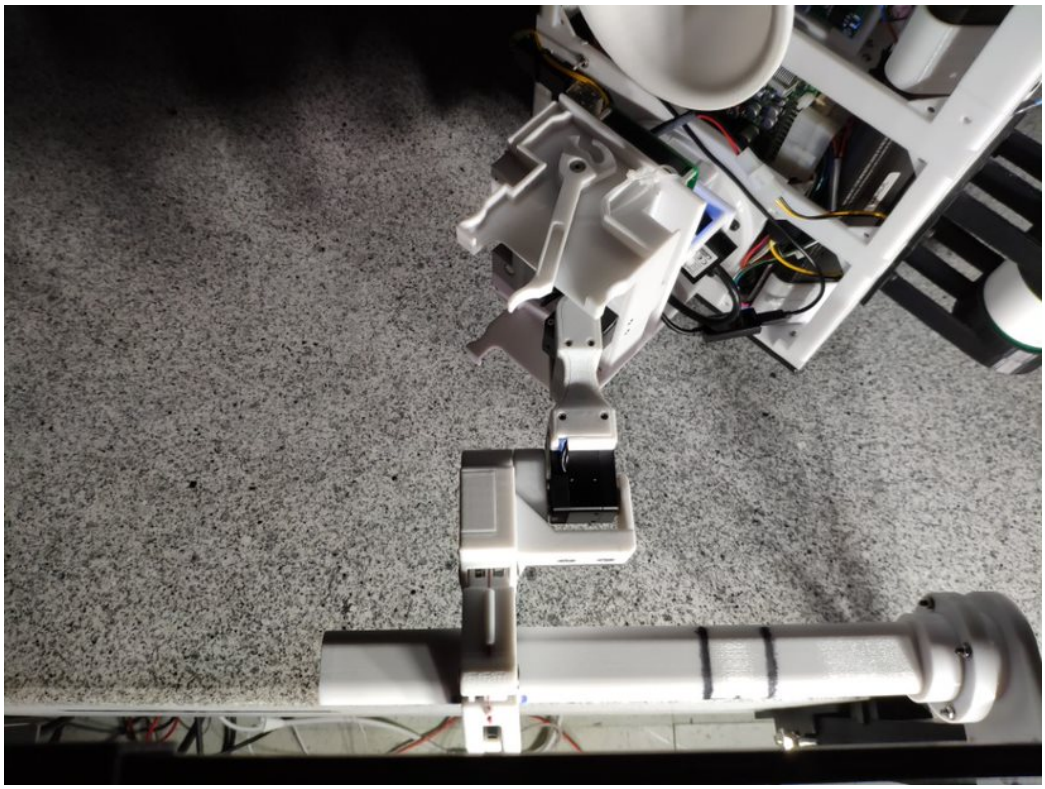

Figure 24. Top down view of proximal joint maneuver set-up.

3. Distal Joint Maneuvers

In order to perform distal joint maneuvers, the perching arm assembly had to be removed from the FSS, rotated 90 degrees, and re-integrated using the 3D-printed adapter plate. In addition, an adapter had to be designed for the ISS handrail in order to place it in a vertical position. The same POSEIDYN procedures for laboratory set-up and shutdown were followed.

Table 3 shows the range of initial and final joint angles that were tested. Maneuvers ending with a release angle of 45 degrees or -45 degrees were excluded from this first round of testing because it was assumed these would result in collisions with the testbed wall, in addition to infeasible maneuvers such as 0 degrees to 0 degrees, which are marked in red.

Table 3. NPS distal joint experiments

		Final Distal Goal (°)						
		-45	-30	-15	0	15	30	45
Initial Distal Angle (°)	45							
	0							
	-45							

Legend	
	Valid
	Not applicable
	Outside Scope

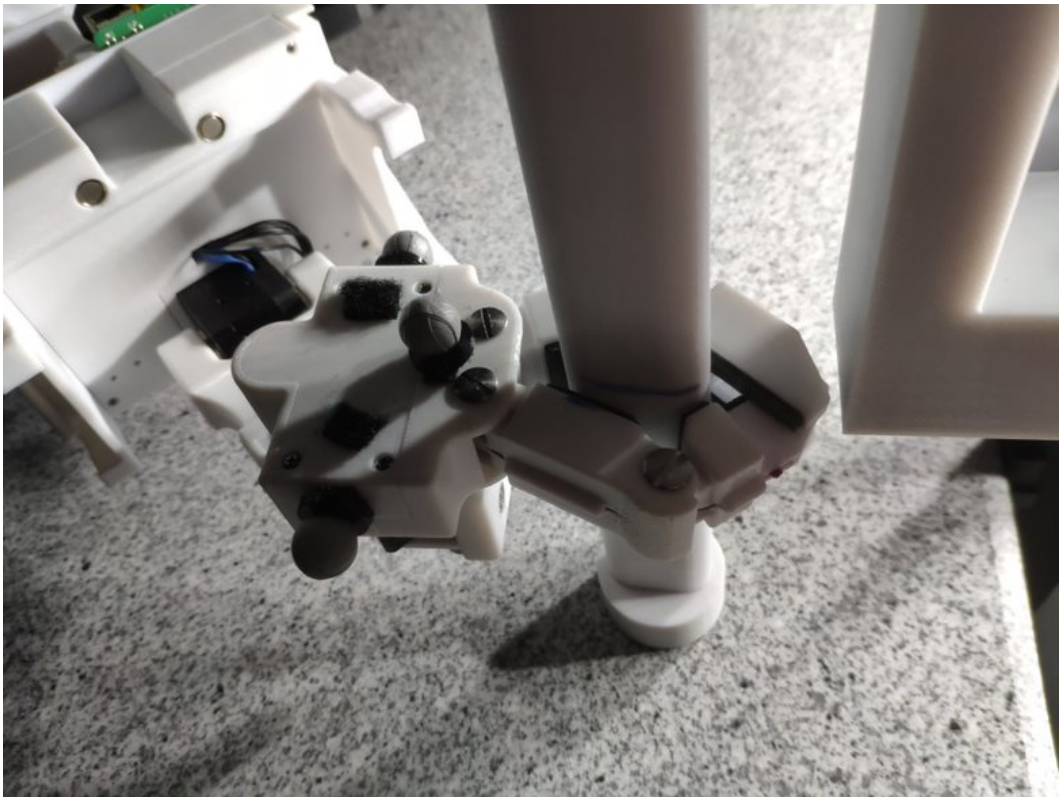

Figure 25. Side view of distal joint maneuver setup.

B. NASA AMES EXPERIMENTS

1. Procedure

Experiments at NASA ARC were quite different from experiments run on POSEIDYN. As discussed in Chapter II, the Granite Lab does not feature a motion tracking system, and all telemetry is collected from the test unit, which is a fully operational Astrobee free-flyer. The range of maneuvers to be tested was sent to ARC before a group from SRL travelled to Mountain View to assist with experimentation. The software was uploaded to the guest science APK within Astrobee's HLP, and a laboratory assistant prepared the test unit for experimentation.

Instead of a single compressed air tank, the base structure for the Astrobee test unit has two replaceable and refillable compressed CO_2 cannisters. These were replaced frequently throughout the course of the day. Another attendant monitored the ground station, which consisted of a single computer with the Astrobee program's user software

initialized. From this workspace, every maneuver already uploaded to the guest science APK can be executed individually. The Astrobee is visualized at the ground station in a ROS (Robot Operating System) Gazebo environment, and the telemetry from the vehicle is recorded in rosbags for post-processing. A rosbag is a file format that stores ROS simulation data. After experimentation is complete, an IRG representative must send the data over NASA's secure network to the Astrobatics team for analysis.

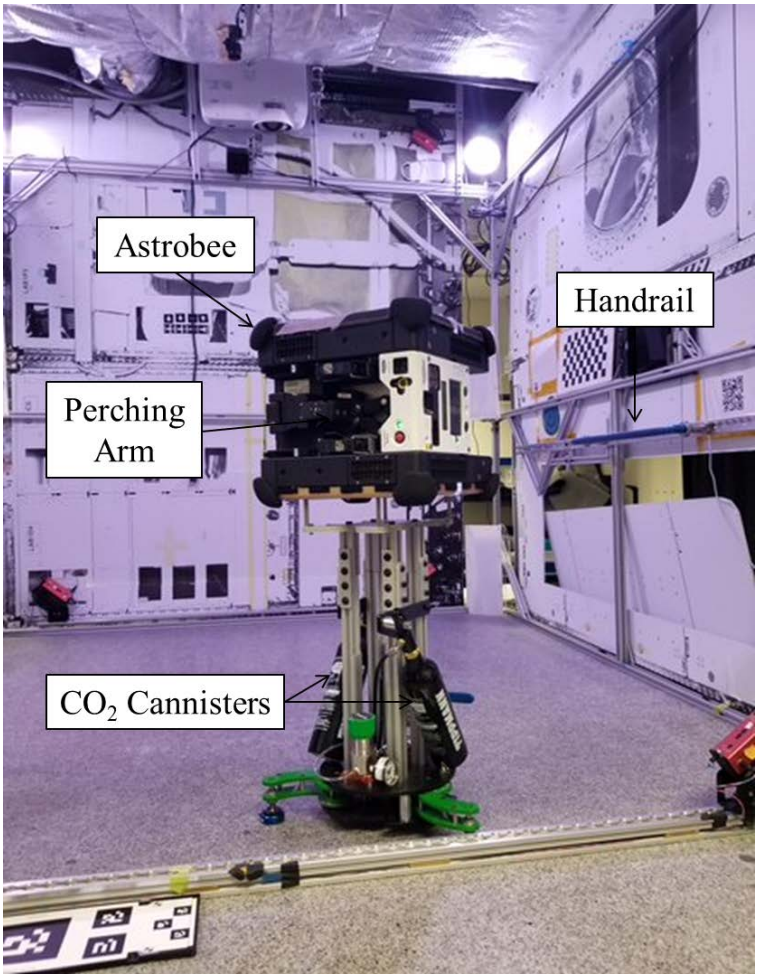

Figure 26. Granite Lab with Astrobee test unit at NASA ARC

2. Proximal Joint Maneuvers

The first round of testing completed at NASA ARC was done using the proximal joint. However, the Astrobatics team opted not to test the same maneuvers already performed at NPS. Those maneuvers will be tested at a later date, but the group wanted to investigate more angular ranges, including a few that are outside the operational limit of Astrobee. When NASA ARC reopens, Astrobatics will return to complete the rest of its proximal testing in addition to all distal maneuvers.

Table 4. NASA ARC proximal joint experiments

		Final Proximal Goal (°)						
			60	75	90	105	120	
Initial Proximal Angle (°)	45	Outside Scope	Valid	Valid	Valid	Valid	Valid	Outside Scope
	90	Outside Scope	Valid	Valid	Not applicable	Valid	Valid	Outside Scope
	135	Outside Scope	Valid	Valid	Valid	Valid	Valid	Outside Scope

Legend	
	Valid
	Not applicable
	Outside Scope

V. EXPERIMENTAL ANALYSIS

A. NPS POST-PROCESSING

The telemetry recorded by the Vicon motion tracking system was processed and analyzed following experimentation. The purpose of this analysis was two-fold: determine which joint produced better launching conditions, and which initial and final angle states those conditions corresponded to. Maneuvers will be identified by a simple naming convention throughout this chapter: ["initial joint angle"i_"final joint angle"f](proximal/distal). For example, a proximal joint maneuver with an initial joint angle of 30 degrees and a release angle of 75 degrees will be referred to as a [30i_75f]p maneuver and a distal joint maneuver with an initial joint angle of -45 degrees and a release angle of -30 degrees will be referred to as a [-45i_-30f]d maneuver.

In order to visualize the results, a MATLAB script was written to produce plots for each initial angle and their associated final angles. It was also important that each plot include all runs of an individual experiment so that reliability could be determined. The FSS base and the perching arm module and manipulator were plotted to show the progression of the vehicle through each maneuver. The wall of the testbed and the replica ISS handrail were plotted for additional convenience. Plots were also generated for x-displacement over time, y-displacement over time, and angular position of the FSS base over time.

Any maneuvers that resulted in minimal motion or collisions with the surface the vehicle was launched from are deemed to be **Failures**. **Partial success** is defined as any maneuver that results in motion away from the handrail wall but with noticeable variation in final position between each run. Thus, **Successful** maneuvers are defined similarly, but with minimal variation between final positions. Following the results section of each joint, the success rate will be summarized in tabular form.

1. Proximal Results

The results for proximal self-toss maneuvers at NPS are presented below in Figure 27-Figure 29. For an initial condition of 30 degrees in the proximal frame, two maneuvers, [30i_60f]p degrees and [30i_75f]p, were successful. The [30i_75f]p maneuver was the most consistent of these two successful experiments with minimal separation between each of its three runs.

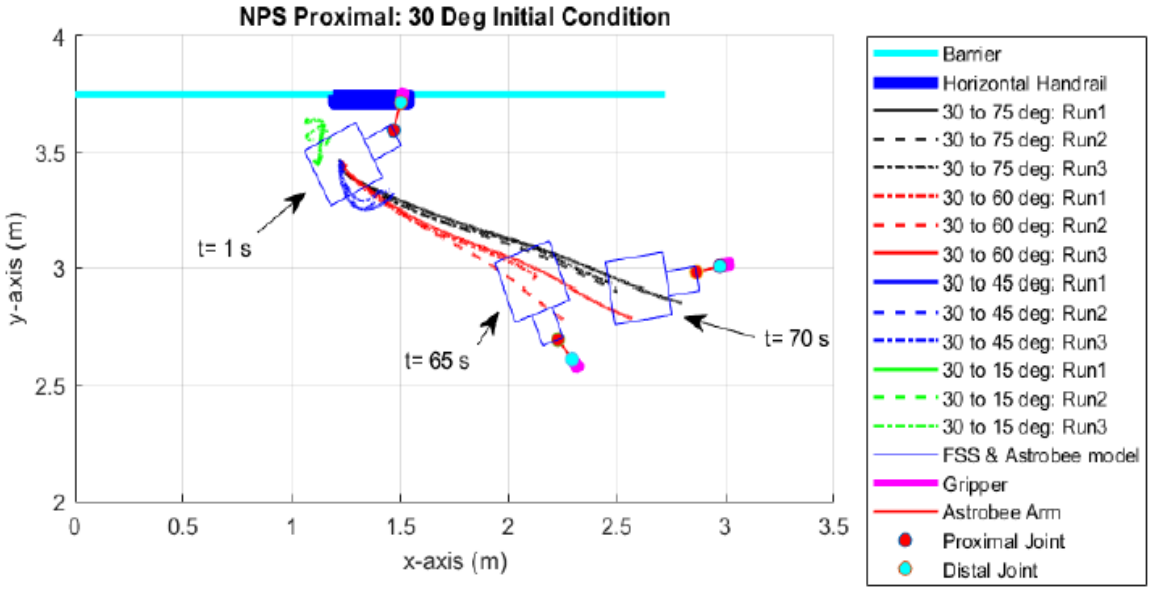

Figure 27. NPS proximal joint results from 30-degree initial angle

Figure 28 shows the maneuvers conducted with an initial condition of 45 degrees. Only one maneuver, [45i_75f]p was successful, while the other three resulted in collisions with the handrail wall.

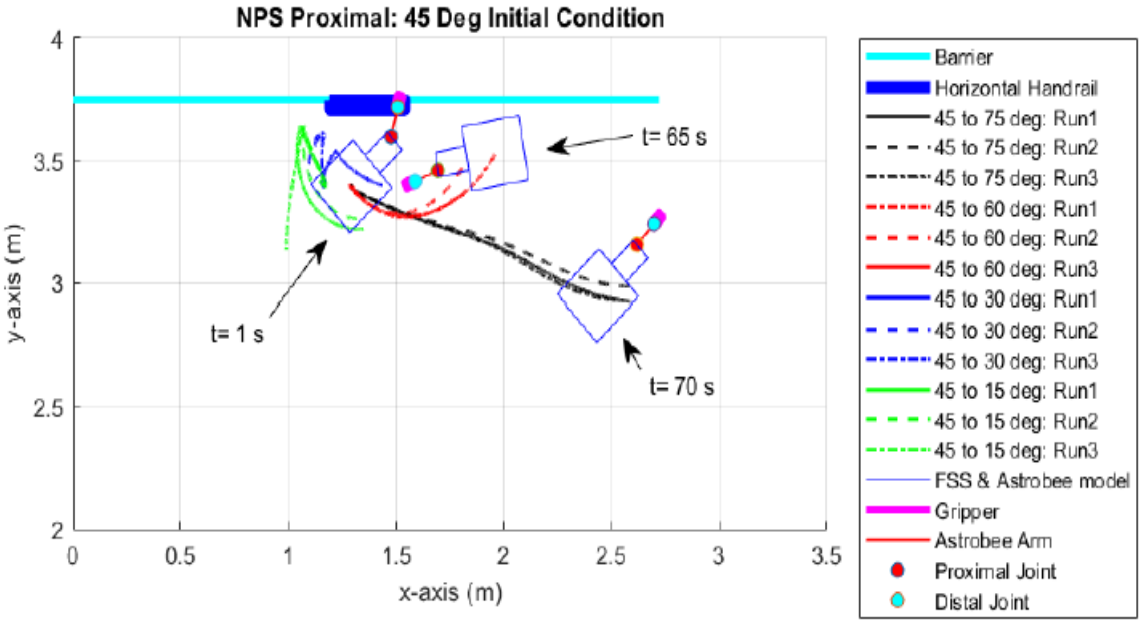

Figure 28. NPS proximal joint results from 45-degree initial angle

Figure 29 displays the results of proximal maneuvers performed with an initial condition of 60 degrees. Every maneuver with this initial condition was a failure; they all impacted with the handrail wall.

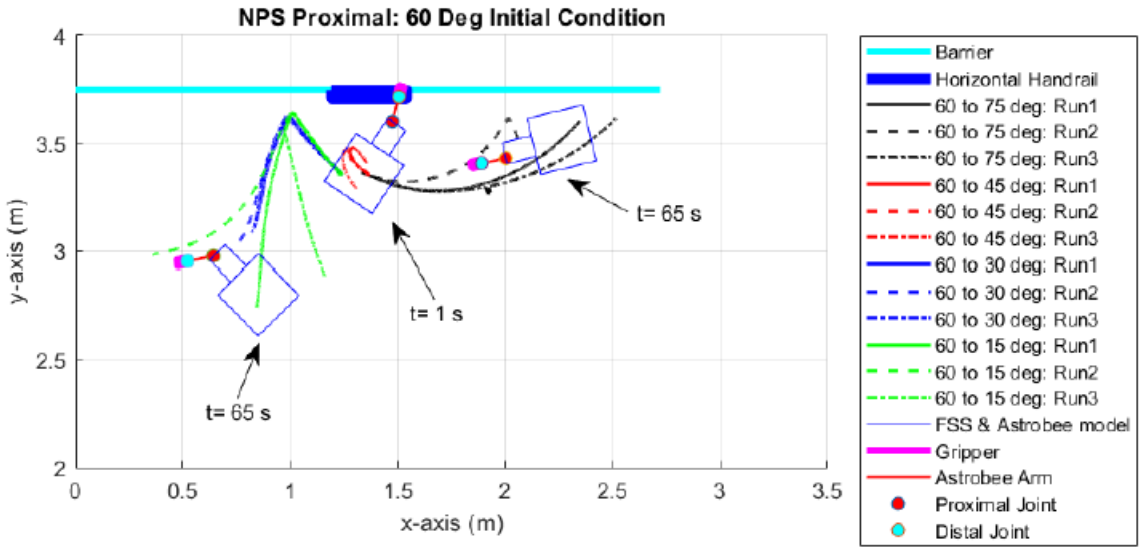

Figure 29. NPS proximal joint results from 60-degree initial angle

Table 5 summarizes the results of the proximal self-toss maneuvers. The only successful maneuvers were performed with an initial joint angle of 30 or 45 degrees, and the maneuver had to actuate through an arc at least 30 degrees. Small maneuvers (>30 degrees) or maneuvers that sent the FSS in the -x direction were all unsuccessful.

Table 5. NPS proximal joint maneuver successes, partial successes, and failures

		Final Proximal Goal (°)				
		15	30	45	60	75
Initial Proximal Angle (°)	30					
	45					
	60					

Legend	
	Success
	Partial Success
	Failure
	Not applicable

More proximal results were acquired in a subsequent session in order to match the experimental campaign at NASA ARC detailed in Chapter IV. Three initial angles were studied: 45 degrees, 90 degrees, and 135 degrees. Two of the maneuvers tested at the Granite Lab, [45i_60f]p and [45i_75f]p, had already been tested previously with POSEIDYN and were excluded from this new round of proximal experiments. These results are displayed in Figures 30–32.

Figure 30 displays the results of additional maneuvers performed with an initial angle of 45 degrees. Two maneuvers, [45i_75f]p and [45i_90f]p, were successful, with [45i_105f]p resulting in a partial success. [45i_105f]p provided the vehicle a great deal of linear momentum, but it cannot be deemed a full success due to its close proximity to the handrail wall through the majority of its trajectory. The other two maneuvers were unsuccessful.

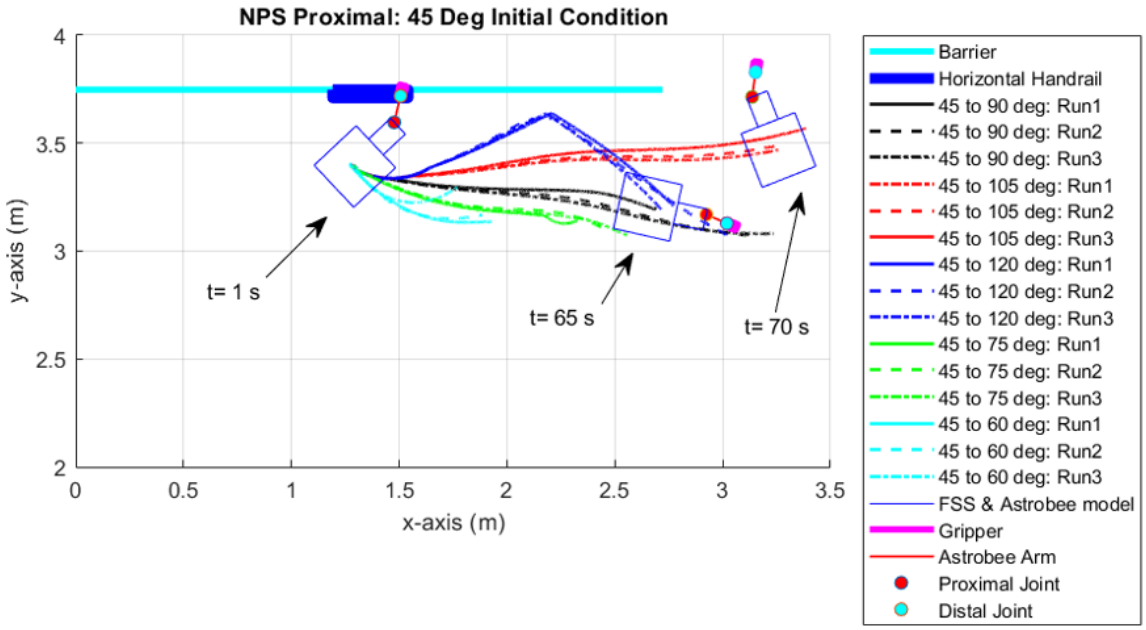

Figure 30. NPS proximal joint results from 45-degree initial angle

Maneuvers initiated with a 90-degree angle were entirely unsuccessful (Figure 31). They either impacted the handrail wall or resulted in minimal motion.

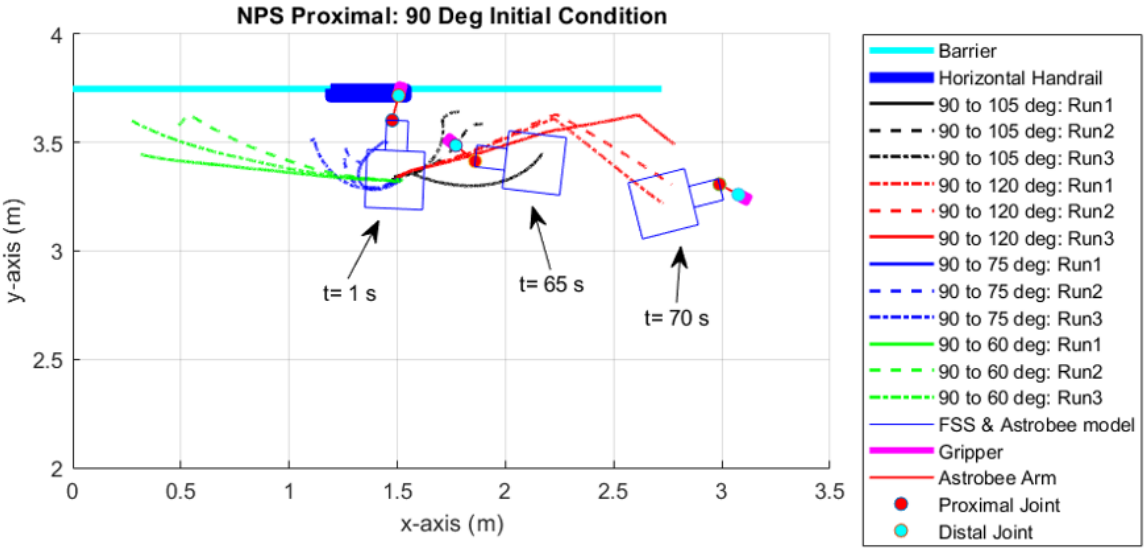

Figure 31. NPS proximal joint results from a 90-degree initial angle

There was one successful maneuver ([135i_90f]p) for maneuvers with an initial angle of 135 degrees (Figure 32). Two maneuvers ([135i_105f]p and [135i_120f]p) showed potential, in that they moved away from the handrail and were consistent, but the total distance travelled was trivial, so they were deemed failures along with the maneuvers that impacted the handrail wall.

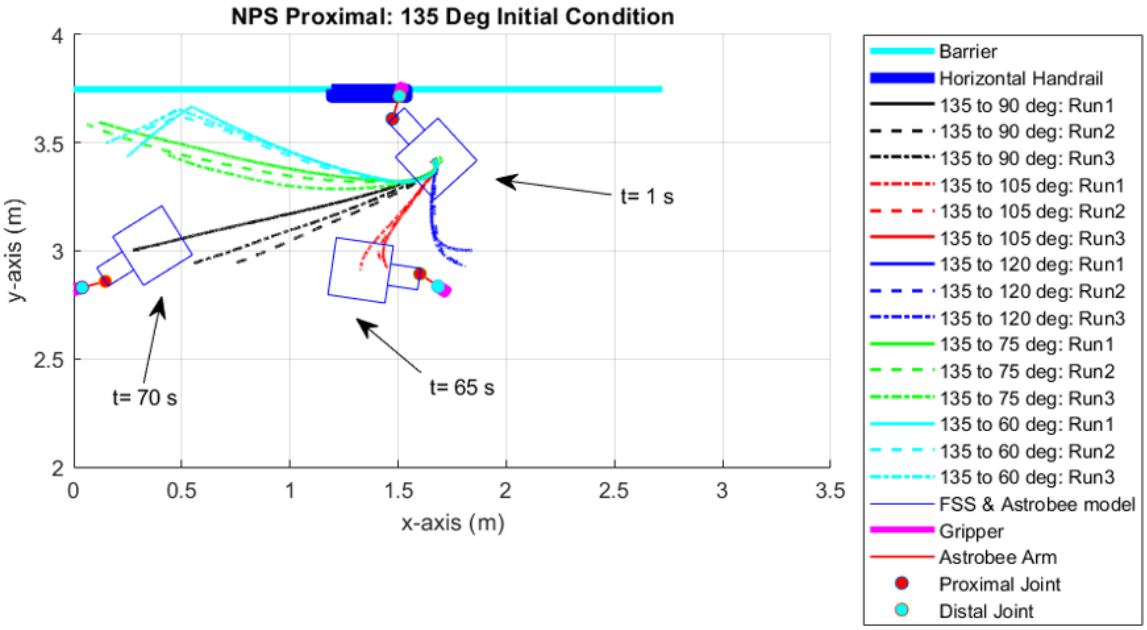

Figure 32. NPS proximal joint results from a 135-degree initial angle

Table 6 summarizes the results of this second round of proximal testing at NPS. Once again, the most successful maneuvers were characterized by large (>30 degree) angular deflections. No maneuver beginning with a 90-degree initial angle was successful.

Table 6. NPS proximal joint maneuver successes, partial successes, and failures, 2nd experimental sequence

Initial Proximal Angle (°)	Final Proximal Goal (°) 60	75	90	105	120
45					
90					
135					

Legend
Success
Partial Success
Failure
Not applicable

2. Distal Results

Distal joint experimental results are shown in Figures 33–35. The replica handrail has been plotted in its vertical state, and the gripper is visualized with its fingers open. Figure 33 shows the results for maneuvers started at 0 degrees in the distal frame. All four maneuvers with this initial condition were failures because they either impacted the handrail wall, or in the cases of [0i_-15f]d and [0i_-45f]d, they failed to produce any meaningful motion away from the wall.

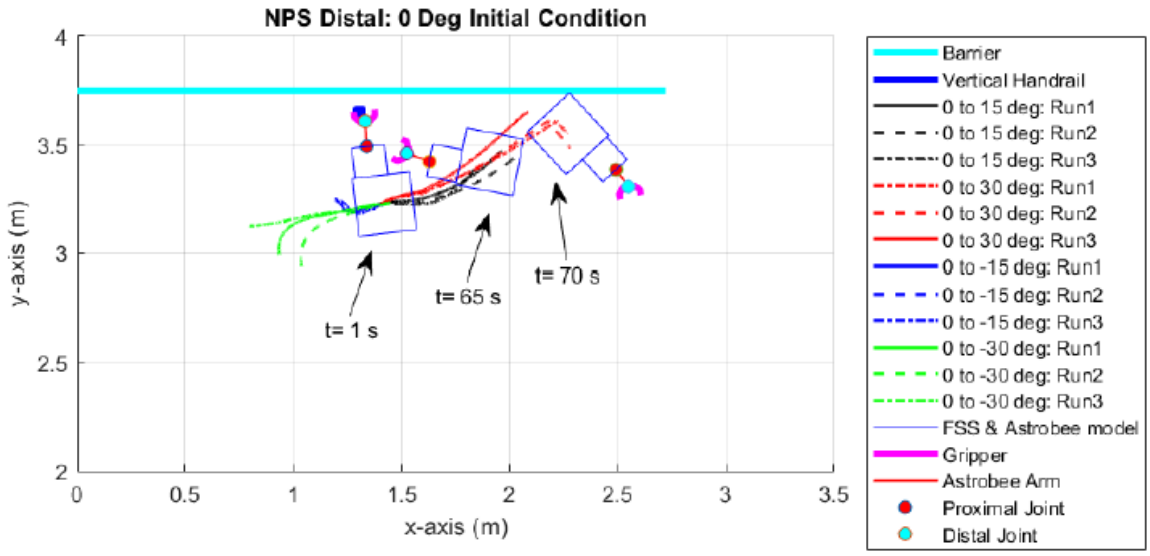

Figure 33. NPS distal joint results from 0-degree initial angle

Figure 34 shows the results of distal maneuvers starting with a 45-degree initial condition. There were two successful experiments [45i_-15f]d and [45i_-30f]d and one partial success [45i_0f]d.

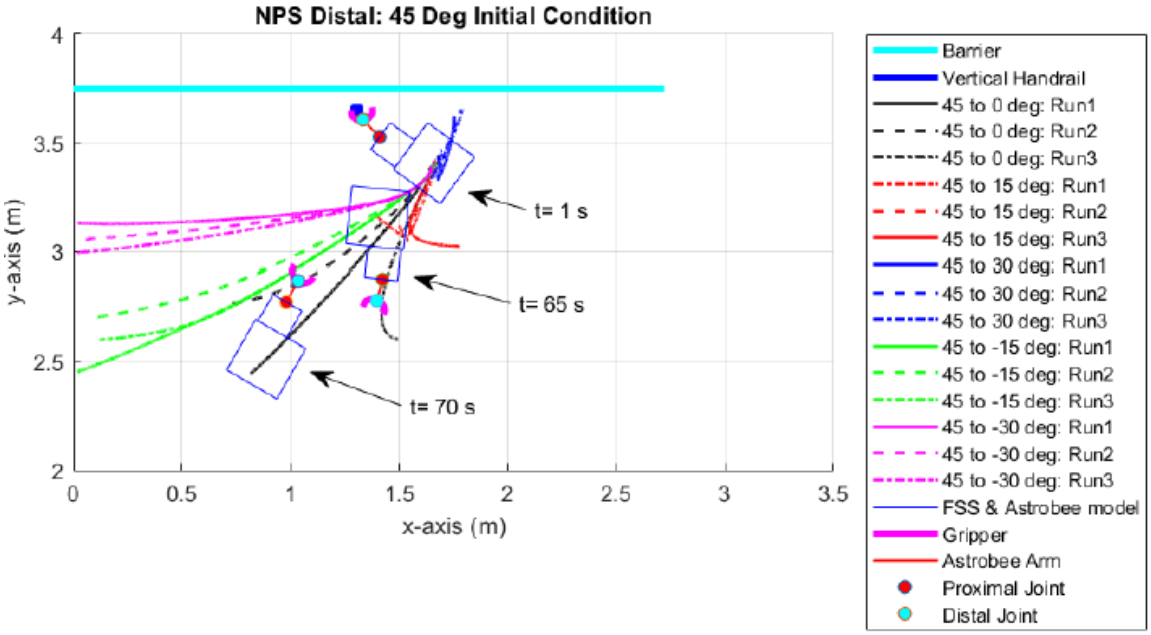

Figure 34. NPS distal joint results from 45-degree initial angle

Figure 35 displays the results for distal maneuvers with a -45-degree initial condition. The [-45i_-30f]d maneuver was a failure, as it did not translate the vehicle very far over 70 seconds and the final position was highly variable among the three runs.

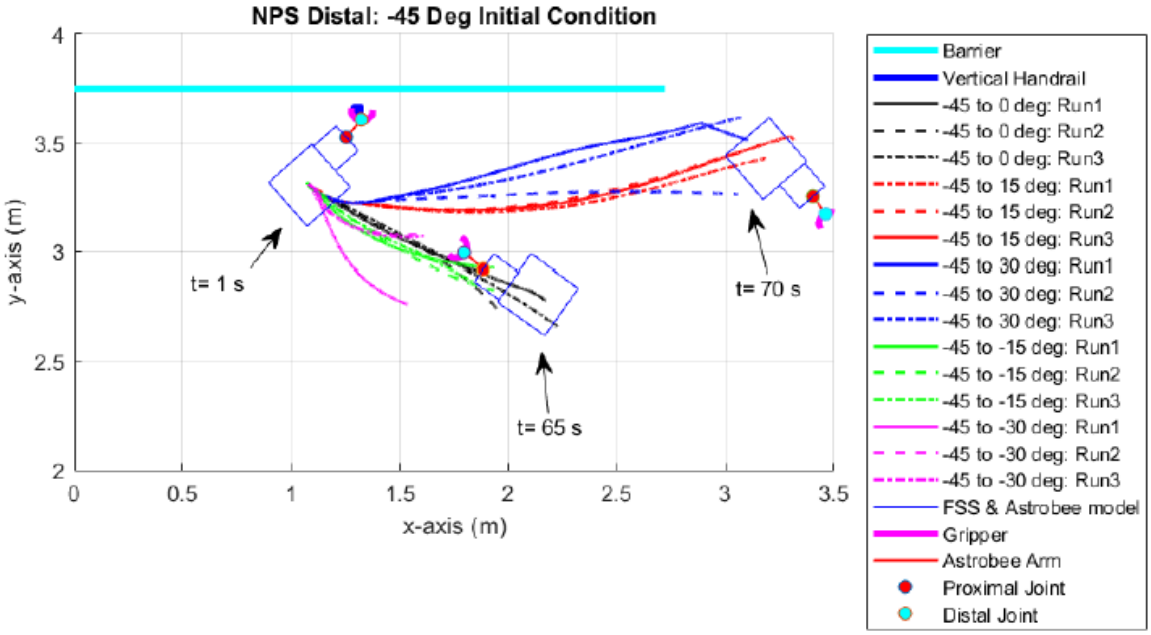

Figure 35. NPS distal joint results from -45-degree initial angle

Table 7 reveals similar behavior to the proximal results in that small angle maneuvers were entirely unsuccessful. Successful maneuvers with an initial condition of 45 degrees had to actuate through at least 45 degrees for a partial success, and greater than or equal to 60 degrees for a successful maneuver.

The most significant failure observed during distal testing was the tendency of the gripper to bounce off the handrail several times before departing. This caused numerous unexpected body forces and torques during the vehicle's motion and led to errant trajectories. It also negated the actuation-developed angular momentum, which further degraded the maneuver. This behavior is to be expected for distal maneuvers because of the way the gripper opens upon final angle release; lateral movement in the FSS base will cause the end effector impact with the side of the handrail when it is vertical. This behavior

is not observed during proximal maneuvers because the gripper fingers never move towards the handrail once released.

Table 7. NPS distal joint maneuver successes, partial successes, and failures

		Final Distal Goal (°)				
		-30	-15	0	15	30
Initial Distal Angle (°)	45					
	0					
	-45					

Legend	
	Success
	Partial Success
	Failure
	Not applicable

B. NASA ARC POST-PROCESSING

Telemetry from the Astrobee test unit was provided to SRL in a compressed file consisting of multiple rosbags. The telemetry from these rosbags was extracted via a MATLAB script which converted the positional data into Cartesian coordinates for plotting and visualization. The Astrobee body and the perching arm were visualized for plotting so that the vehicle's progression could be observed.

No distal results have been acquired from the Granite Lab yet, but a comparative study of overlapping proximal results from both NPS and NASA ARC will be presented later in this section.

1. Proximal Results

Three initial angles were investigated at Granite Lab during the first round of proximal testing: 45, 90, and 135 degrees. As discussed in Chapter IV, the majority of the proximal maneuvers tested at NASA ARC had not been tested previously at NPS.

Figure 36 displays the results of maneuvers conducted with an initial angle 0f 45 degrees. The maneuvers [45i_75f]p and [45i_90f]p produced the most consistent results, while [45i_60f]p resulted in the most distance away from the handrail. Its first run may have been affected by depleted CO_2 tanks, so this maneuver is worth investigating further.

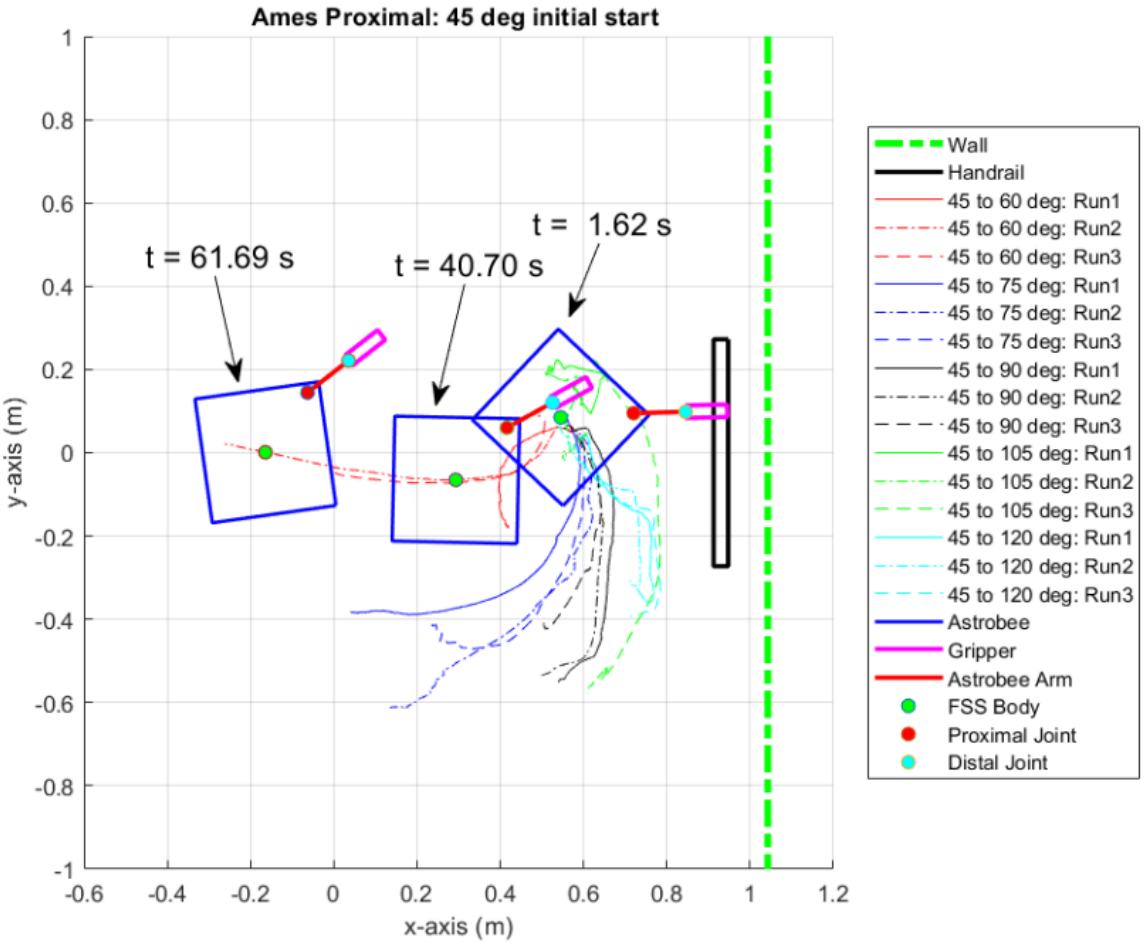

Figure 36. ARC proximal joint results from a 45-degree initial angle

Figure 37 depicts the results of maneuvers performed from a 90-degree initial angle. [90i_60f]p and [90i_75f]p were successful in that they resulted in meaningful motion away from the handrail. Surprisingly, the most successful maneuver, [90i_75f]p, had an angular deflection of only 15 degrees, which has not been observed in most maneuvers. The erratic motion in all three runs of [90i_60f]p suggests testing conditions were not consistent during this experiment, because regardless of launch velocity, the trajectories should be smooth assuming a frictionless surface.

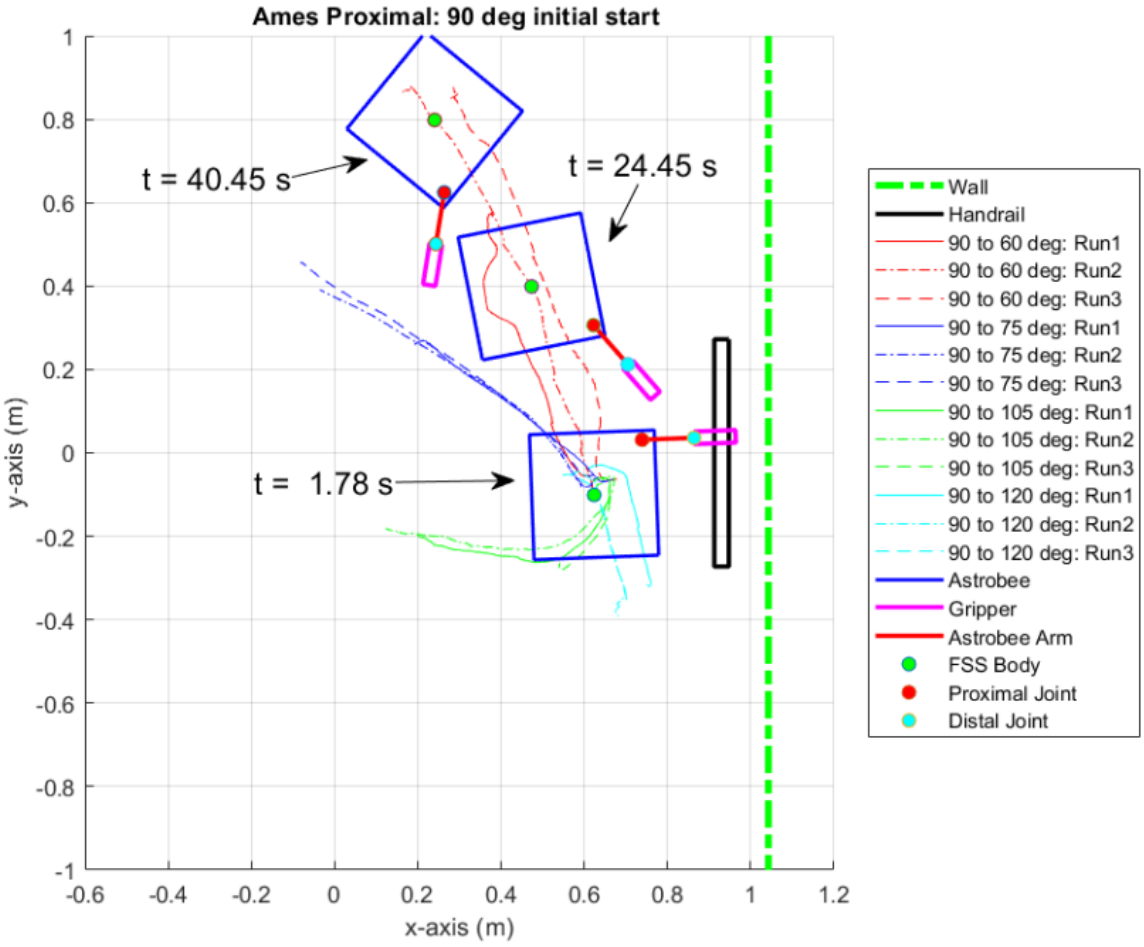

Figure 37. ARC proximal joint results from a 90-degree initial angle

The most successful initial angle observed at NASA ARC was 135 degrees (Figure 38). Only one maneuver failed, and predictably, it consisted of a small angular deflection

([135i_120f]p). The most interesting feature of this initial angle is how similar the trajectories are regardless of release angle. The proximal joint is technically not supposed to operate in this angular range, but the results are promising and invite further investigation pending approval from the Astrobee development team.

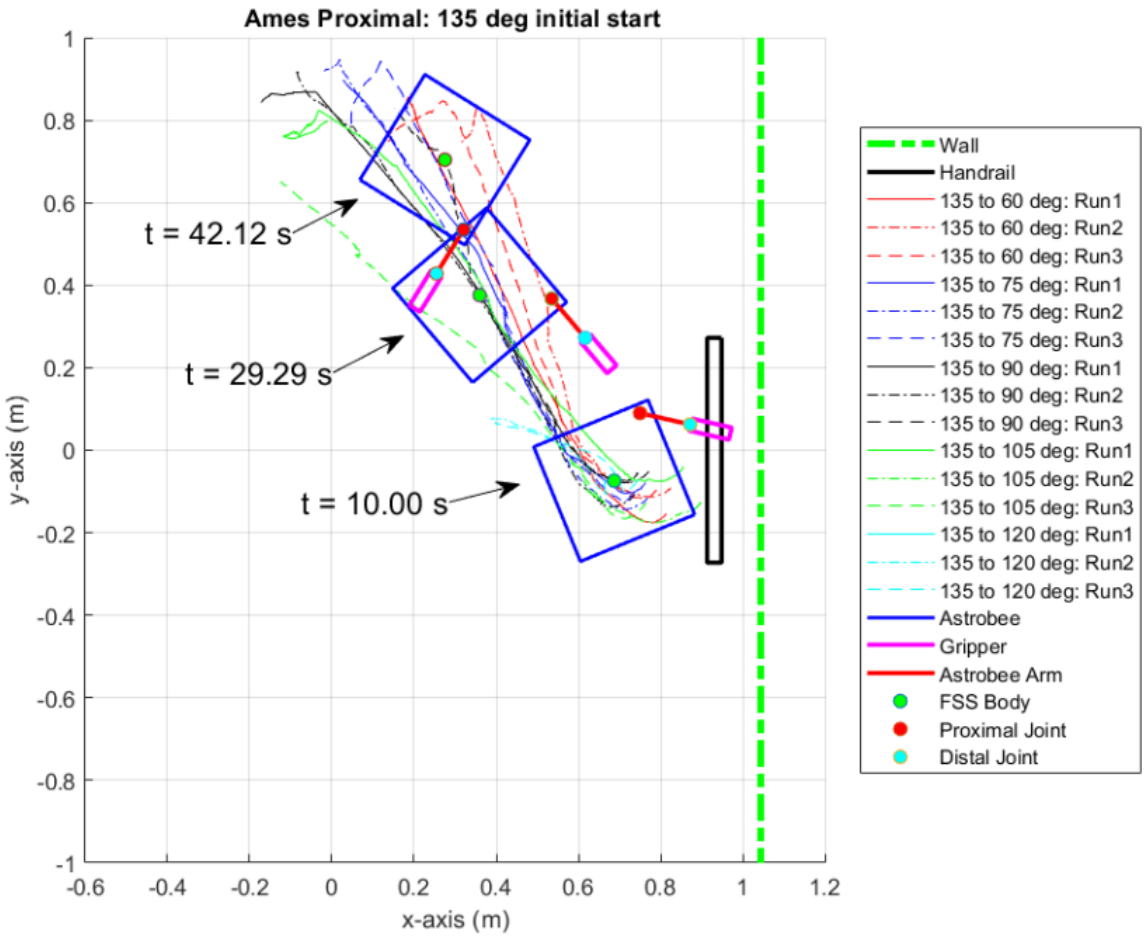

Figure 38. ARC proximal joint results from a 135-degree initial angle

More experiments need to be conducted at NASA ARC in order to fully characterize the ability of the proximal joint to execute self-toss maneuvers. Table 8 summarizes the results from the first round of testing using the Granite Lab. Only one maneuver with a deflection less than 30 degrees was successful ([90i_75f]p), while all other successful maneuvers had large angular deflections. This appears to confirm the conclusion from POSEIDYN data that large angular deflections result in optimal launching conditions.

Table 8. ARC proximal joint maneuver successes, partial successes, and failures

		Final Proximal Goal (°)				
		60	75	90	105	120
Initial Proximal Angle (°)	45					
	90					
	135					

Legend	
	Success
	Partial Success
	Failure
	Not applicable

2. NPS and NASA ARC Comparative Study

A plotting script was written to overlay the Ames results with the NPS POSEIDYN results (Appendix B). Due to the dynamic differences between the POSEIDYN FSS and the Granite Lab Astrobee test unit, the vehicles respond differently to impulses and their trajectories can be quite different. Several successful maneuvers were plotted with this script and they are presented below. As only the trajectories were analyzed for these plots, their corresponding vehicle bodies were not visualized. To reiterate, the plots visualize the trajectories of the FSS base and Astrobee test unit geometric center, not the center of mass for either system. Most of the compared maneuvers are presented in Appendix A, but some are shown below in Figures 39-44 to illustrate some concerning discrepancies between the data. The following results suggest there is not much correlation between maneuvers with the same initial and final joint angles when carried out by the two different test platforms.

a. 45-degree Initial Angle

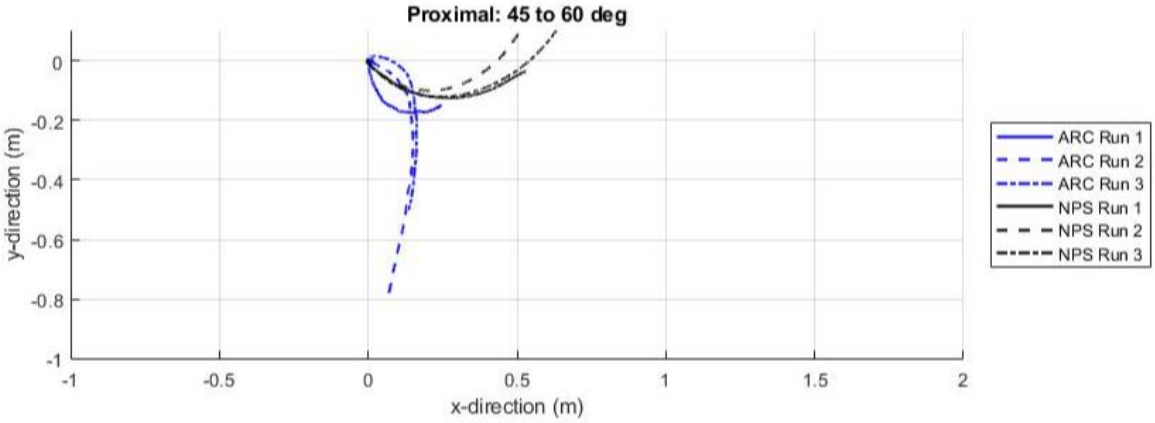

Figure 39. NPS and NASA ARC comparative study of [45i_60f]p

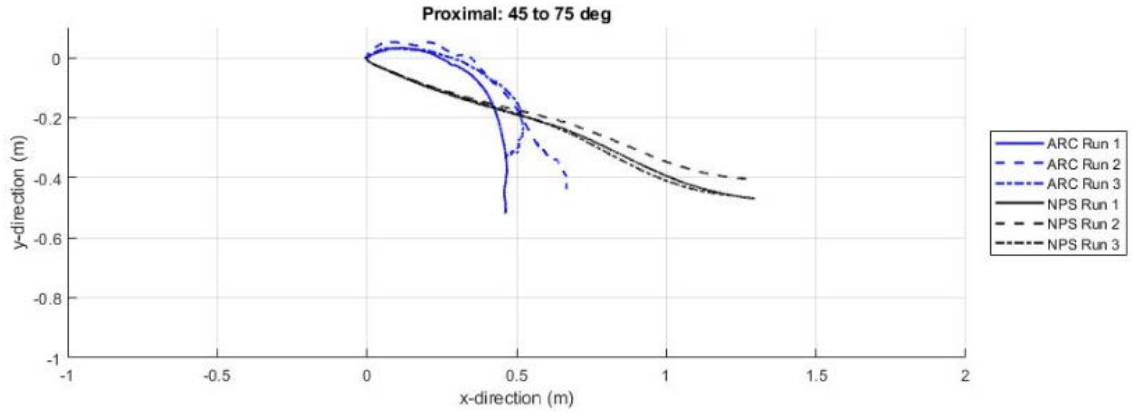

Figure 40. NPS and NASA ARC comparative study of [45i_75f]p

b. 90-degree Initial Angle

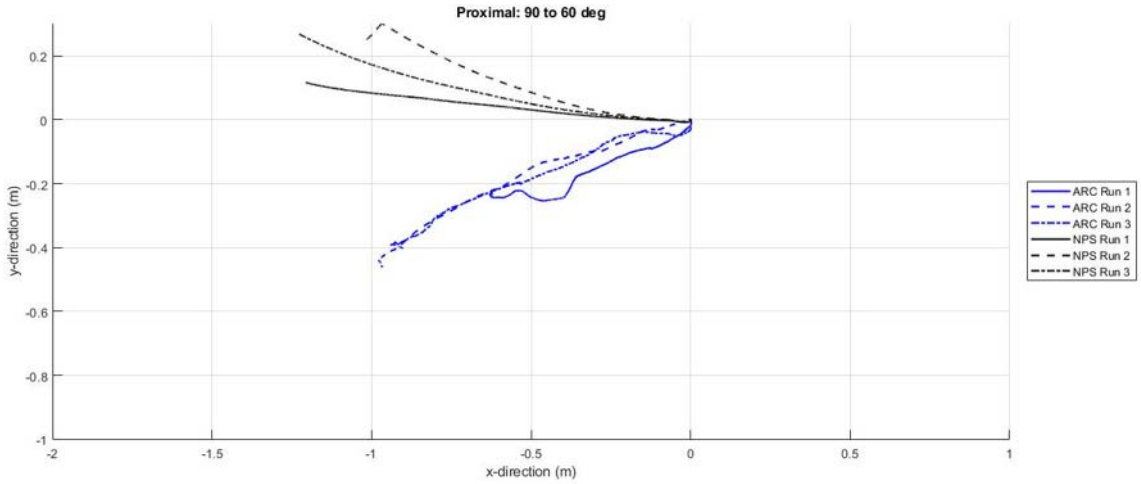

Figure 41. NPS and NASA ARC comparative study of [90i_60f]p

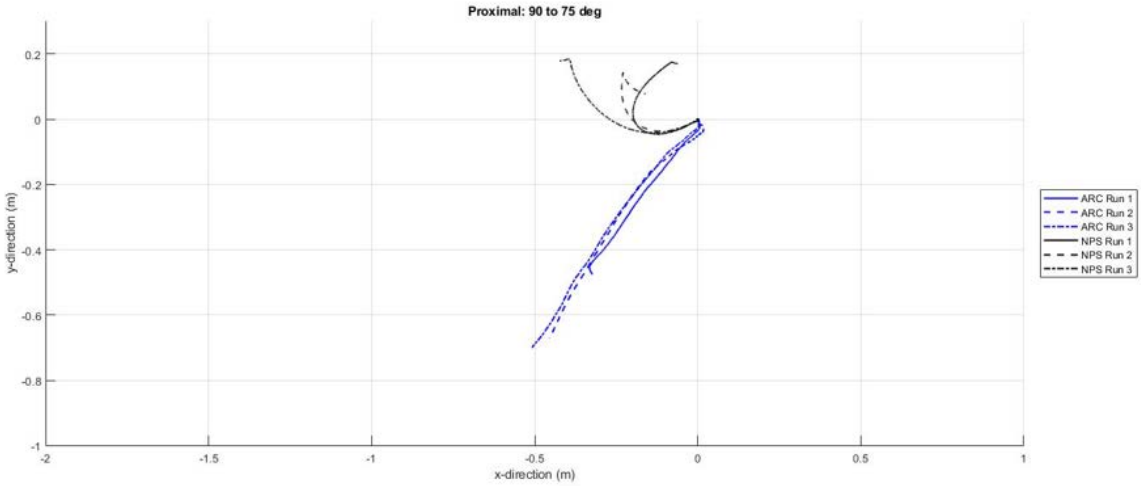

Figure 42. NPS and NASA ARC comparative study of [90i_75f]p

c. 135-degree Initial Angle

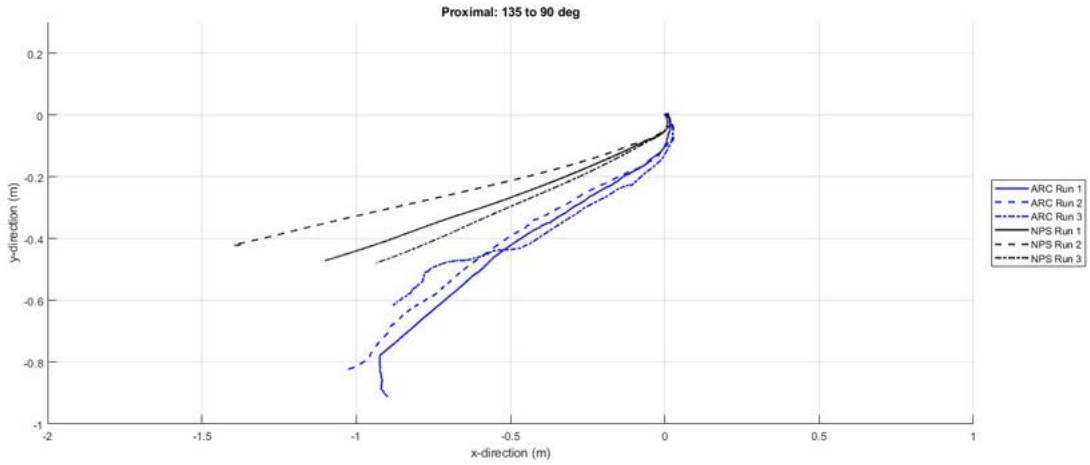

Figure 43. NPS and NASA ARC comparative study of [135i_90f]p

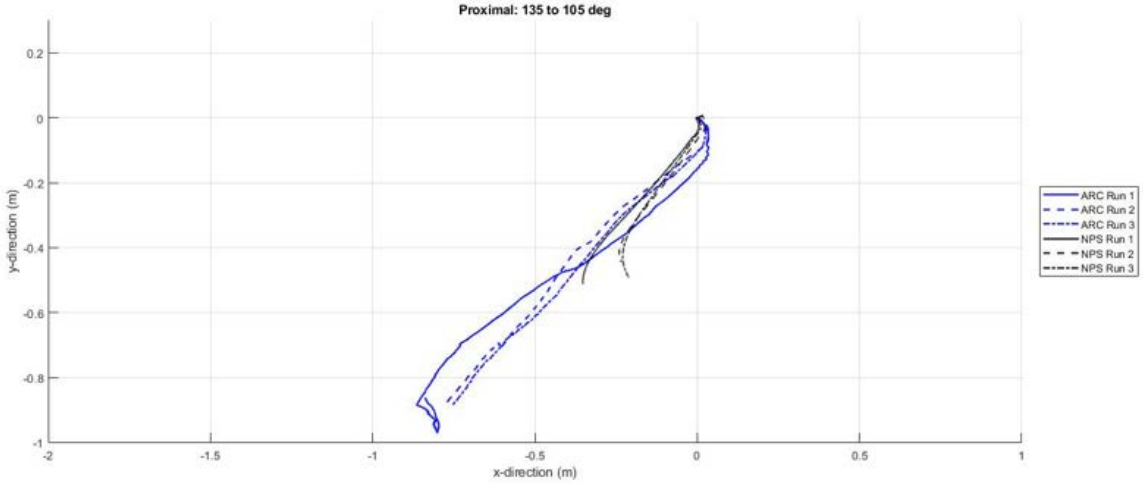

Figure 44. NPS and NASA ARC comparative study of [135i_105f]p

It is evident that there are many inconsistencies between POSEIDYN and Granite Lab experimentation. The floating base of the Astrobee test unit appeared to suffer from drag during some experiments. The vehicle displayed errant behavior during some maneuvers and it was observed that the base would pivot around one of the three air-bearings. This could have been caused by a partially closed valve that prevented the air-

bearing from being fully pressurized, or the CO_2 tanks may have depleted quicker than anticipated.

The two systems are dynamically quite different, and this most likely had the greatest effect on the variability of the results. The extruded perching arm module on the POSEIDYN FSS base gave the platform a larger moment arm during maneuvers compared to the Astrobee test unit where the perching arm is situated much closer to the system's center of mass. Due to similarity of the Astrobee test unit to the flight vehicle that will be used during ISS experimentation, these results show that testing on POSEIDYN alone is not sufficient for testing beyond S1.

Interestingly, maneuvers conducted with a 135-degree initial angle were mostly successful, and the POSEIDYN and Granite Lab data largely agree. This initial angle technically exists outside of the defined operational range of the proximal joint, but it may be worth investigating this initial condition further and requesting an exception during ISS experimentation. NASA ARC experimentation also proved that large angular deflections provide the best launching conditions, regardless of their correlation with POSEIDYN data.

VI. CONCLUSIONS

A. SUMMARY OF RESULTS

Most of the experimentation that SRL desired to be conducted prior to the S1 self-toss maneuver onboard the ISS has been completed. Maneuvers were tested with a variety of initial and final conditions on both the proximal and distal joints. Both joints were tested at NPS and their corresponding maneuvers were plotted and analyzed. The maneuvers were compared with the purpose of determining if the proximal or distal joint provided better launching conditions, in addition to what initial and final joint angles produced those maneuvers.

Preliminary results suggest that maneuvers with angular deflections of 30-45 degrees provide the best results for proximal joint maneuvers, and 45-60 degrees for distal joint maneuvers. More work must be done to determine why this is the case, but it is likely that the vehicle simply does not develop enough linear momentum to carry it through a full maneuver if the joint actuation is too small.

An answer to the question of which joint provides the best launching conditions is going to require more data at this stage. To date, no distal joint maneuvers have been attempted at NASA ARC with the Astrobee test unit. However, it appears that many distal maneuvers suffer from handrail-gripper impacts immediately upon release. These impacts affect the reliability of distal maneuvers and will certainly influence which joint is preferred. Due to the geometry of the perching arm gripper, it is believed that these effects will be observed during distal testing at NAS ARC.

A comparative study of NPS POSEIDYN and NASA ARC Granite Lab experiments yielded conflicting results. The trajectories of the vehicles are very different when subjected to the same angular deflections. Some of this may be attributed to the dynamic differences between the FSS and the Astrobee test unit, but testing conditions may have also affected the results. There were noticeable moments of drag during Granite Lab testing where the vehicle seemed to pivot around a single air-bearing. Future Granite Lab experiments will require more scrutiny to ensure optimal testing conditions. The most

promising initial angle in the proximal frame during NPS and ARC testing was 135 degrees, despite existing outside the defined operational range. Not only were these maneuvers successful, their trajectories observed at both NPS and at ARC closely aligned.

B. FUTURE WORK

The most immediate task for SRL is to complete any outstanding S1 maneuver tests at NASA ARC. These include a few remaining proximal maneuvers and all distal maneuvers that have been tested at NPS but not in the Granite Lab (Table 9). While it does appear from initial testing with POSEIDYN that the proximal joint will provide the best launching conditions for the vehicle, it is worth confirming this conclusion with additional data using a fully operational Astrobee. As aforementioned, more care shall be taken to ensure consistent testing conditions are consistent throughout experimentation.

Table 9. Proximal maneuvers to be completed at NASA ARC

Initial Proximal Angle (°)	Final Proximal Goal (°)						
	0	15	30	45	60	75	90
30	Outside Scope	SRL only	Not applicable	SRL only	SRL only	SRL only	Outside Scope
45	Outside Scope	SRL only	SRL only	Not applicable	SRL and ARC	SRL and ARC	Outside Scope
60	Outside Scope	SRL only	SRL only	SRL only	Not applicable	SRL only	Outside Scope

Legend
SRL only
SRL and ARC
Not applicable
Outside Scope

Beyond the completion of S1 ground testing, SRL must prepare for its first ISS experiment. This will involve the development of crew procedures that astronauts can follow, which will first require the approval of NASA Johnson Space Center, the location of Mission Control for the ISS. SRL also plans to build a ground station that it can use to directly communicate with and record data from Astrobee while it is performing self-toss maneuvers. Depending on crew time delays, this could be operational before the on-orbit S1 experiment.

SRL will have to closely investigate Astrobee's control subsystem once it is prepared to begin S2 experimentation. Stabilization of the vehicle will require the use of its 12 thrusters, so an intense understanding of the control logic will be a prerequisite, especially since Astrobee will be experiencing large linear and angular velocity profiles. A full dynamic model simulator is in development, and this will assist SRL in this endeavor. This model will track the trajectory of the entire system's center of mass, which according to theory should propagate in a straight line towards the destination handrail upon gripper release. Control of the actuation will have to shift from commanding a final angle to commanding a linear and angular velocity from which the control subsystem chooses an appropriate torque to apply to the joint and an angle to release the gripper.

C. RESEARCH SIGNIFICANCE

Robotic hopping maneuvers could contribute to space exploration in ways that are not currently known or conceivable. Expanding capabilities in space beyond the limitations of propellant will allow new discoveries and enable longer duration activities. In addition to increased IVA capabilities, future ISS robots could assume some of the time-consuming EVAs that current astronauts must perform to maintain the aging research platform. This would not only protect the astronauts from EVA-related incidents, but also maximize their time to perform on-orbit research. Hopping spacecraft could also revolutionize the field of on-orbit diagnostics and servicing of satellites; instead of carrying out costly propulsion-limited proximity operations, a small spacecraft could just as easily use an onboard robotic arm manipulator to hop between satellite components. As with much space research, the potential benefits of robotic hopping will likely emerge in exciting and totally unexpected applications.

THIS PAGE INTENTIONALLY LEFT BLANK

APPENDIX A.

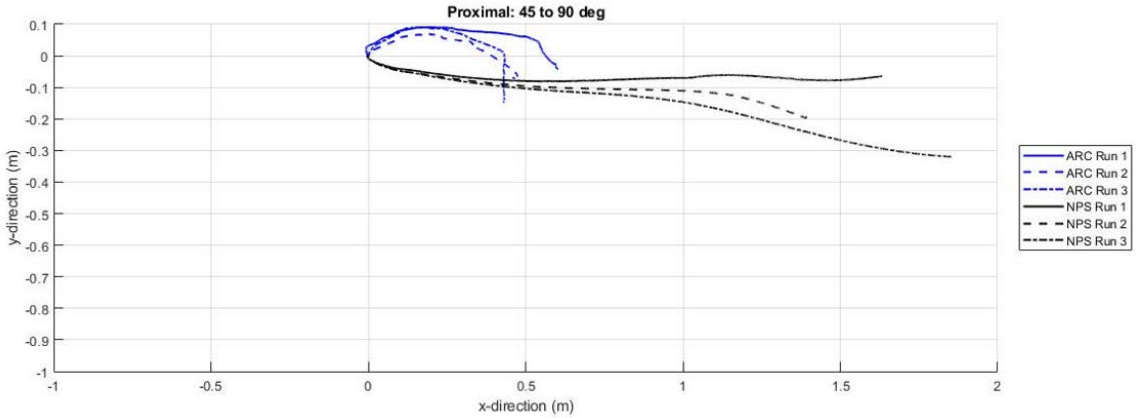

Figure 45. NPS and NASA ARC comparative study of [45i_90f]p

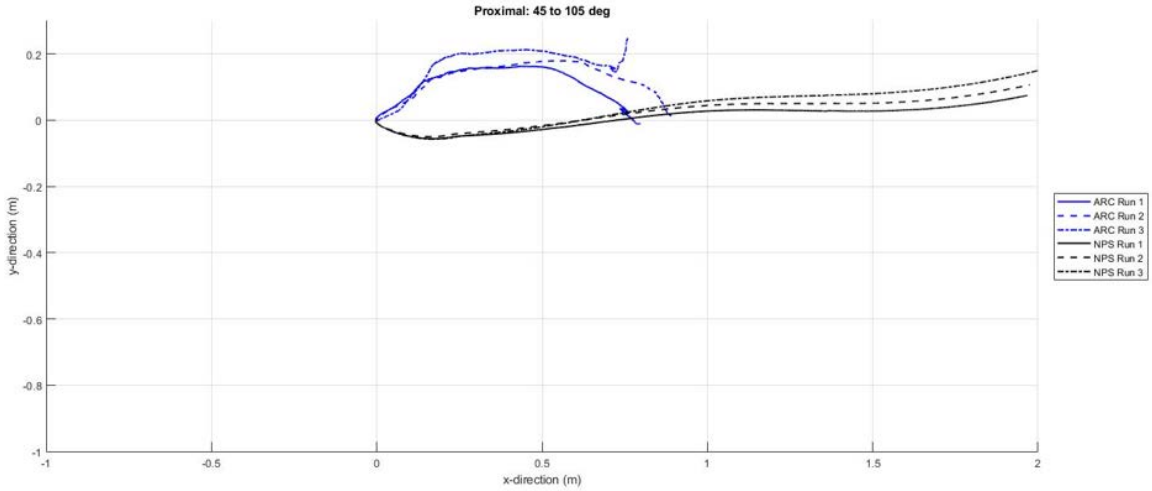

Figure 46. NPS and NASA ARC comparative study of [45i_105f]p

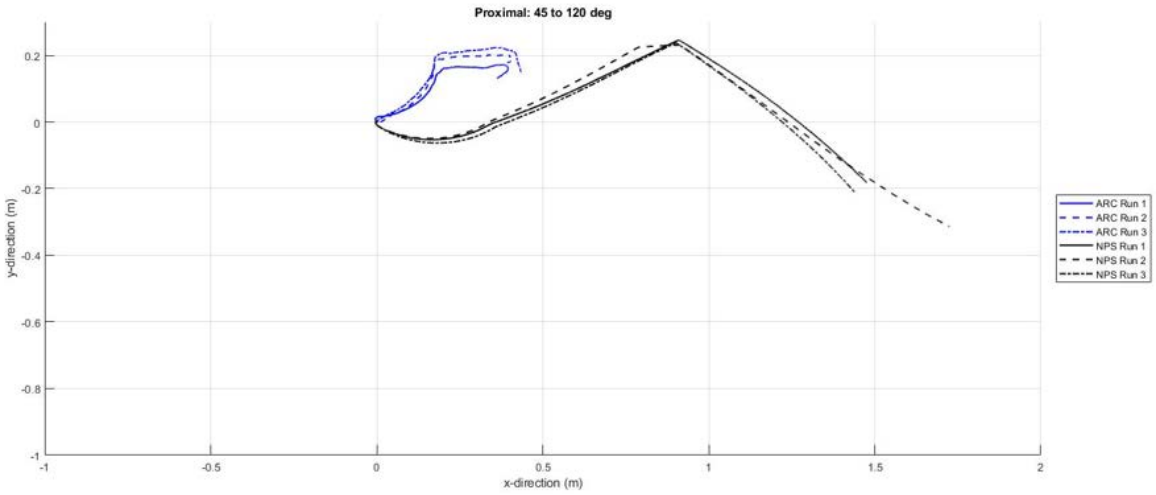

Figure 47. NPS and NASA ARC comparative study of [45i_120f]p

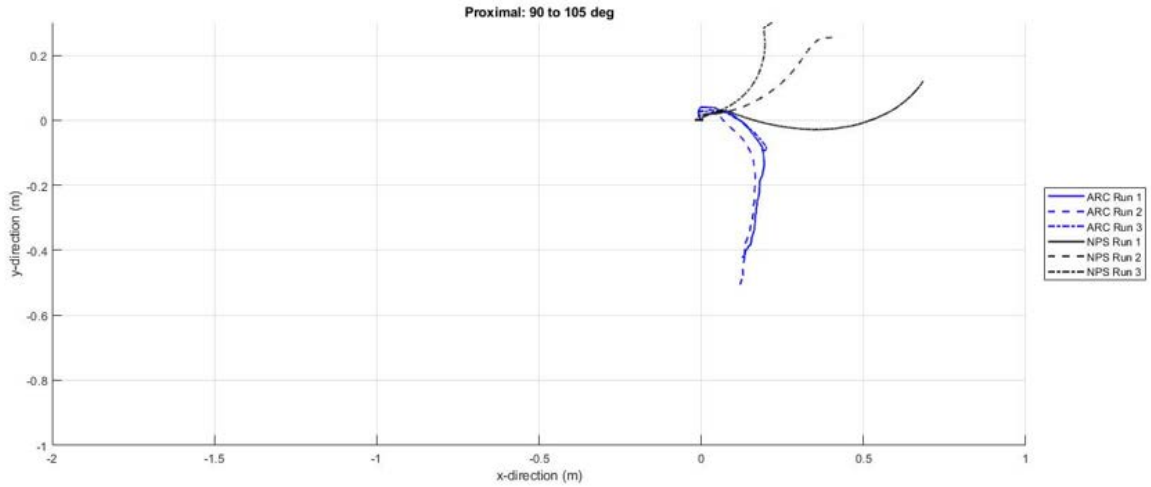

Figure 48. NPS and NASA ARC comparative study of [90i_105f]p

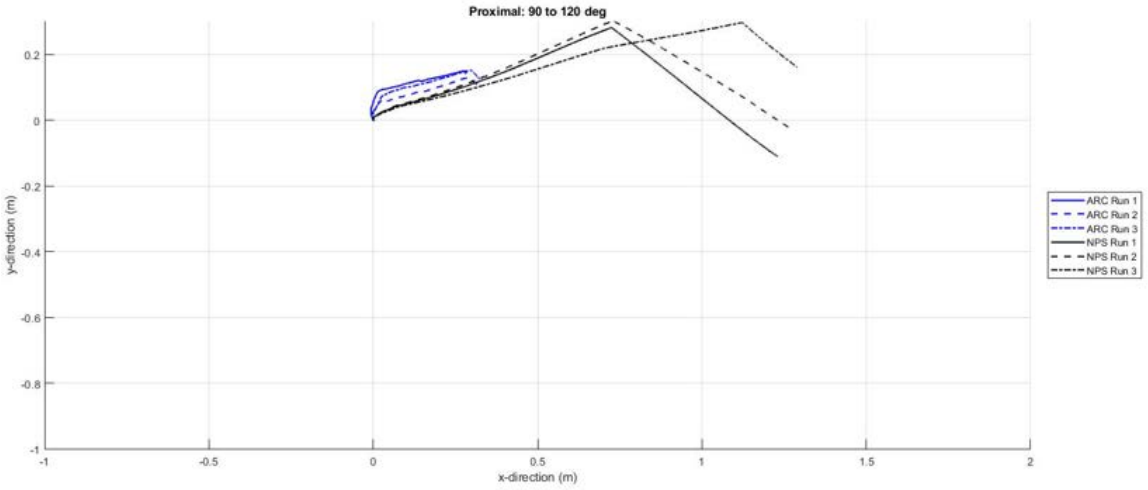

Figure 49. NPS and NASA ARC comparative study of [90i_120f]p

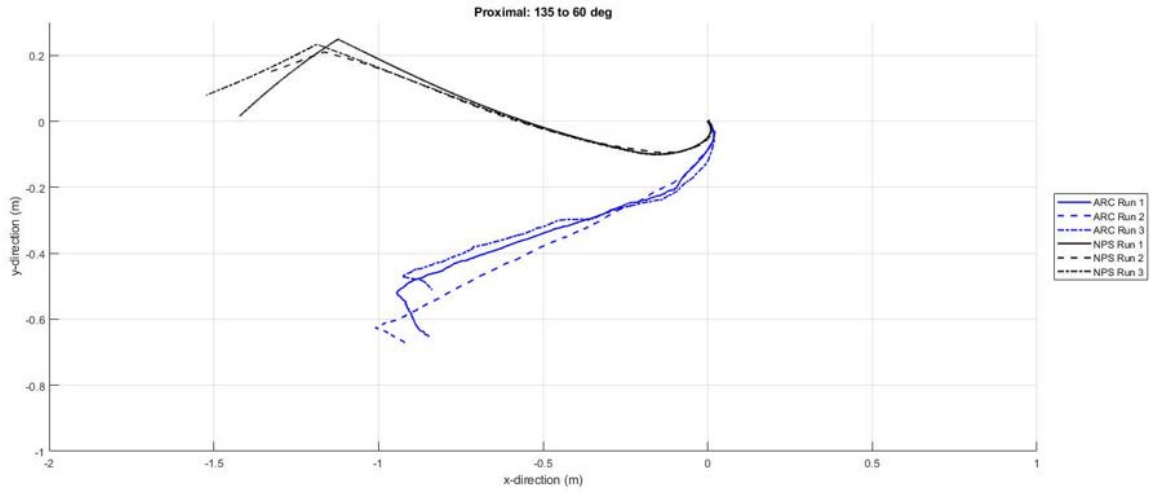

Figure 50. NPS and NASA ARC comparative study of [135i_60f]p

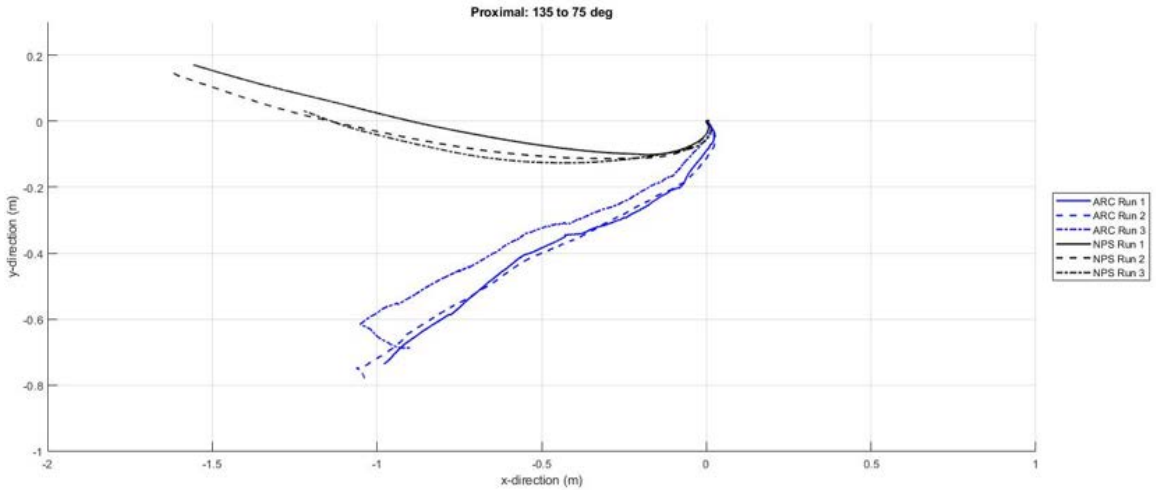

Figure 51. NPS and NASA ARC comparative study of [135i_75f]p

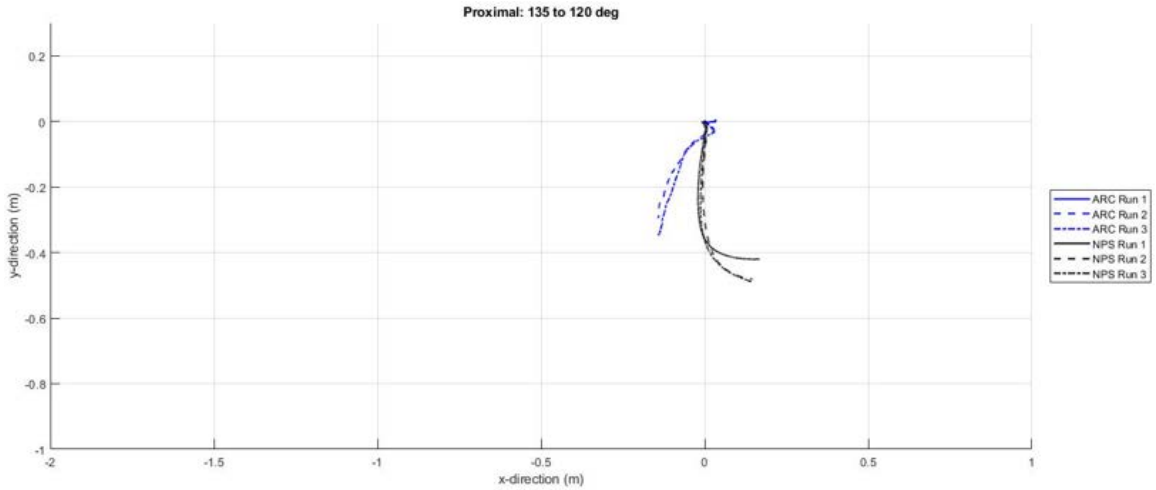

Figure 52. NPS and NASA ARC comparative study of [135i_120f]p

APPENDIX B.

```
clear all
close all
clc

%Script written by Stephen Kwok Choon and Conor Safbom to extract
rosbag
% dataset and compare it to corresponding POSEIDYN dataset
% MAY 20 2020

% To write this script example code was taken from matlab documentation
% https://www.mathworks.com/help/ros/ug/work-with-rosbag-logfiles.html
% https://www.mathworks.com/help/ros/ref/rosbag.html

bag1 = rosbag('20160211_2040_nps_135_120_r1_0.bag');%extract data run 1
bag2 = rosbag('20160211_2042_nps_135_120_r2_0.bag');%extract data run 2
bag3 = rosbag('20160211_2043_nps_135_120_r3_0.bag');%extract data run 3

t_start1 = bag1.StartTime; %clock start time
t_end1 = bag1.EndTime; %clock end time

t_start2 = bag2.StartTime; %clock start time
t_end2 = bag2.EndTime; %clock end time

t_start3 = bag3.StartTime; %clock start time
t_end3 = bag3.EndTime; %clock end time

%topics = bag1.AvailableTopics

%% select a particular dataset from NASA Ames
%
% %bag 1
%
bSel_astate1 = select(bag1, 'Time', [t_start1 t_end1], 'Topic',
'/beh/arm/arm_state');
bSel_jstates1 = select(bag1, 'Time', [t_start1 t_end1], 'Topic',
'/joint_states');
bSel_ekf1 = select(bag1, 'Time', [t_start1 t_end1], 'Topic',
'/gnc/ekf');
bSel_pose1 = select(bag1, 'Time', [t_start1 t_end1], 'Topic',
'/loc/pose');
%
% % Read messages as a structure. Specify the DataFormat name-value
pair when
% % reading the messages. Inspect the first structure in the returned
cell
% % array of structures.
%
msgStruct_astate1 = readMessages(bSel_astate1,'DataFormat','struct');
msgStruct_jstates1 = readMessages(bSel_jstates1,'DataFormat','struct');
msgStruct_ekf1 = readMessages(bSel_ekf1,'DataFormat','struct');
```

```
msgStruct_pose1 = readMessages(bSel_pose1,'DataFormat','struct');

msgStruct_astate1{1};
msgStruct_jstates1{1};
msgStruct_ekf1{1};
msgStruct_pose1{1};
%
% %bag 2
%
bSel_astate2 = select(bag2, 'Time', [t_start2 t_end2], 'Topic',
'/beh/arm/arm_state');
bSel_jstates2 = select(bag2, 'Time', [t_start2 t_end2], 'Topic',
'/joint_states');
bSel_ekf2 = select(bag2, 'Time', [t_start2 t_end2], 'Topic',
'/gnc/ekf');
bSel_pose2 = select(bag2, 'Time', [t_start2 t_end2], 'Topic',
'/loc/pose');

Read messages as a structure. Specify the DataFormat name-value pair
when reading the messages. Inspect the first structure in the returned
cell array of structures.

msgStruct_astate2 = readMessages(bSel_astate2,'DataFormat','struct');
msgStruct_jstates2 = readMessages(bSel_jstates2,'DataFormat','struct');
msgStruct_ekf2 = readMessages(bSel_ekf2,'DataFormat','struct');
msgStruct_pose2 = readMessages(bSel_pose2,'DataFormat','struct');

msgStruct_astate2{1};
msgStruct_jstates2{1};
msgStruct_ekf2{1};
msgStruct_pose2{1};
%
%%bag 3
%
bSel_astate3 = select(bag3, 'Time', [t_start3 t_end3], 'Topic',
'/beh/arm/arm_state');
bSel_jstates3 = select(bag3, 'Time', [t_start3 t_end3], 'Topic',
'/joint_states');
bSel_ekf3 = select(bag3, 'Time', [t_start3 t_end3], 'Topic',
'/gnc/ekf');
bSel_pose3 = select(bag3, 'Time', [t_start3 t_end3], 'Topic',
'/loc/pose');

Read messages as a structure. Specify the DataFormat name-value pair
when reading the messages. Inspect the first structure in the returned
cell array of structures.

msgStruct_astate3 = readMessages(bSel_astate3,'DataFormat','struct');
msgStruct_jstates3 = readMessages(bSel_jstates3,'DataFormat','struct');
msgStruct_ekf3 = readMessages(bSel_ekf3,'DataFormat','struct');
msgStruct_pose3 = readMessages(bSel_pose3,'DataFormat','struct');

msgStruct_astate3{1};
msgStruct_jstates3{1};
```

```
msgStruct_ekf3{1};
msgStruct_pose3{1};

%%% extract the data into a readable array

%run1
xPoints_r1 = cellfun(@(m) double(m.Pose.Position.X),msgStruct_ekf1);
yPoints_r1 = cellfun(@(m) double(m.Pose.Position.Y),msgStruct_ekf1);

%run2
xPoints_r2 = cellfun(@(m) double(m.Pose.Position.X),msgStruct_ekf2);
yPoints_r2 = cellfun(@(m) double(m.Pose.Position.Y),msgStruct_ekf2);

%run3
xPoints_r3 = cellfun(@(m) double(m.Pose.Position.X),msgStruct_ekf3);
yPoints_r3 = cellfun(@(m) double(m.Pose.Position.Y),msgStruct_ekf3);

%% Read in NPS POSEIDYN data

cd NPS

cd prox_45_30_r1;
load vehicle2.mat; load astrobee;
run1 = vehicle2; astrobee_1 = astrobee;
clear vehicle2; clear astrobee;
cd ..

cd prox_45_30_r2;
load vehicle2;
run2 = vehicle2;
clear vehicle2;
cd ..

cd prox_45_30_r3;
load vehicle2;
run3 = vehicle2;
clear vehicle2;
cd ..

% process sample

v2_run1 = round(run1, 5) ; % round to 5th decimal place
v2_run2 = round(run2, 5) ; % round to 5th decimal place
v2_run3 = round(run3, 5) ; % round to 5th decimal place

astrobee_run1 = round(astrobee_1, 10); % round to 5th decimal place




% Input for element to find
```

```
time_cut_off = 70; %seconds
elementToFind = time_cut_off; %cut off mark, seconds
rowToReturn = 1;
% The algorithm
[tf,colWithElement] = ismember(elementToFind,v2_run1(1,:));
output = v2_run1(rowToReturn,colWithElement);

% %example code to show replacement of '0' values
% lengthvar = length(v2_run1);
% figure(1)
% plot(v2_run1(1,:),v2_run1(3,:))
% ylabel("X value")
% xlabel("Time(s)")

%
lengthvar = length(v2_run1);

for i = 5:lengthvar

 %correcting x value
 if (v2_run1(3,i) == 0)
 %disp('check');
 v2_run1(3,i) = v2_run1(3,i-1);
 end

 %correcting y value0
 if (v2_run1(4,i) == 0)
 %disp('check');
 v2_run1(4,i) = v2_run1(4,i-1);
 end

 %correcting phi value
 if (v2_run1(5,i) == 0)
 %disp('check');= v2_run1_0_30(5,i); % specific phi value
 v2_run1(5,i) = v2_run1(5,i-1);
 end

end

lengthvar2 = length(v2_run2);

for i = 5:lengthvar2

 %correcting x value
 if (v2_run2(3,i) == 0)
 %disp('check');
 v2_run2(3,i) = v2_run2(3,i-1);
 end

 %correcting y value

 if (v2_run2(4,i) == 0)
```

```
 %disp('check');
 v2_run2(4,i) = v2_run2(4,i-1);
 end

 %correcting phi value
 if (v2_run2(5,i) == 0)
 %disp('check');= v2_run1_0_30(5,i); % specific phi value
 v2_run2(5,i) = v2_run2(5,i-1);
 end

end

lengthvar3 = length(v2_run3);

for i = 5:lengthvar3

 %correcting x value
 if (v2_run3(3,i) == 0)
 %disp('check');
 v2_run3(3,i) = v2_run3(3,i-1);
 end

 %correcting y value
 if (v2_run3(4,i) == 0)
 %disp('check');
 v2_run3(4,i) = v2_run3(4,i-1);
 end

 %correcting phi value
 if (v2_run3(5,i) == 0)
 %disp('check');= v2_run1_0_30(5,i); % specific phi value
 v2_run3(5,i) = v2_run3(5,i-1);
 end


end

lengthvar4 = length(astrobee_run1);

%cleaning function for astrobee arm
for i = 5:lengthvar4

 %correcting x value
 if (astrobee_run1(2,i) == 0)
 %disp('check');
 astrobee_run1(2,i) = astrobee_run1(2,i-1);
 end

 %correcting y value
 if (astrobee_run1(3,i) == 0)
 %disp('check');
 astrobee_run1(3,i) = astrobee_run1(3,i-1);
 end
```

```
 %correcting z value
 if (astrobee_run1(4,i) == 0)
 %disp('check');
 astrobee_run1(4,i) = astrobee_run1(4,i-1);
 end


 %correcting phi value
 if (astrobee_run1(5,i) == 0)
 %disp('check');
 astrobee_run1(5,i) = astrobee_run1(5,i-1);
 end

 %correcting psi value
 if (astrobee_run1(6,i) == 0)
 %disp('check');
 astrobee_run1(6,i) = astrobee_run1(6,i-1);
 end

 %correcting phi value
 if (astrobee_run1(7,i) == 0)
 %disp('check');
 astrobee_run1(7,i) = astrobee_run1(7,i-1);
 end
end

%% Plotting of Data

Ames_x1 = (xPoints_r1-xPoints_r1(1));
Ames_y1 = (yPoints_r1-yPoints_r1(1));
% Run 2 Data
Ames_x2 = xPoints_r2-xPoints_r2(1);
Ames_y2 = yPoints_r2-yPoints_r2(1);
% Run 3 Data
Ames_x3 = xPoints_r3-xPoints_r3(1);
Ames_y3 = yPoints_r3-yPoints_r3(1);

% create a matrix of these points, which will be useful in future
calculations
v1 = [Ames_x1 Ames_y1];
v2 = [Ames_x2 Ames_y2];
v3 = [Ames_x3 Ames_y3];
% choose a point which will be the center of rotation
x1_center = Ames_x1(1);
y1_center = Ames_y1(1);
x2_center = Ames_x2(1);
y2_center = Ames_y2(1);
x3_center = Ames_x3(1);
y3_center = Ames_y3(1);
% create a matrix which will be used later in calculations
center1 = repmat([x1_center; y1_center], 1, length(Ames_x1));
center2 = repmat([x2_center; y2_center], 1, length(Ames_x2));
center3 = repmat([x3_center; y3_center], 1, length(Ames_x3));
```

```
% define a 90 degree counter-clockwise rotation matrix
theta = pi/2; % pi/2 radians = 90 degrees
R = [cos(theta) -sin(theta); sin(theta) cos(theta)];
% do the rotation...
s1 = v1' - center1; % shift points in the plane so that the center of
rotation is at the origin
s2 = v2' - center2;
s3 = v3' - center3;
so_1 = R*s1; % apply the rotation about the origin
so_2 = R*s2;
so_3 = R*s3;
vo_1 = so_1 + center1; % shift again so the origin goes back to the
desired center of rotation
vo_2 = so_2 + center2;
vo_3 = so_3 + center3;
% this can be done in one line as:
% vo = R*(v - center) + center
% pick out the vectors of rotated x- and y-data
Ames_x1_rot = vo_1(1,:);
Ames_y1_rot = vo_1(2,:);
Ames_x2_rot = vo_2(1,:);
Ames_y2_rot = vo_2(2,:);
Ames_x3_rot = vo_3(1,:);
Ames_y3_rot = vo_3(2,:);


% make a plot
figure(1)
plot(Ames_x1, Ames_y1, 'k-', Ames_x1_rot, Ames_y1_rot, 'r-', x1_center,
y1_center, 'bo');
axis equal

% NPS Data
% Run 1 Data Normalization
NPS_x1 = v2_run1(3,(1:colWithElement))-v2_run1(3,1);
NPS_y1 = v2_run1(4,(1:colWithElement))-v2_run1(4,1);
% Run 2 Data Normlization
NPS_x2 = v2_run2(3,(1:colWithElement))-v2_run2(3,1);
NPS_y2 = v2_run2(4,(1:colWithElement))-v2_run2(4,1);
% Run 3 Data Normalization
NPS_x3 = v2_run3(3,(1:colWithElement))-v2_run3(3,1);
NPS_y3 = v2_run3(4,(1:colWithElement))-v2_run3(4,1);
```

```
figure(2)

hold on;

grid on;

hold on
plot(Ames_x1_rot,Ames_y1_rot, 'b', 'LineWidth',1.5)
plot(Ames_x2_rot,Ames_y2_rot, '--b', 'LineWidth', 1.5)
plot(Ames_x3_rot,Ames_y3_rot, '-.b', 'LineWidth', 1.5)
hold on
plot(NPS_x1,NPS_y1, 'k', 'LineWidth', 1.5) %trajectory of vehicle
plot(NPS_x2,NPS_y2, '--k', 'LineWidth', 1.5) %trajectory of vehicle
plot(NPS_x3,NPS_y3, '-.k', 'LineWidth', 1.5) %trajectory of vehicle
grid on
hold off

title('Proximal: 135 to 120 deg');
xlabel('x-direction (m)');
ylabel('y-direction (m)');
legend('ARC Run 1', 'ARC Run 2', 'ARC Run 3', 'NPS Run 1', 'NPS Run 2',
'NPS Run 3', 'location','EastOutside')
axis equal
xlim([-2 1])
ylim([-1 0.3])
```

LIST OF REFERENCES

[1] J. Virgili-llop, K. Alsup, J. Komma, and M. Romano, "Analysis and simulation of robotic hopping maneuvers inside the International Space Station with Astrobee," pp. 1–9.

[2] K. Alsup, "Robotic Spacecraft Hopping : Application and analysis," M.S. thesis, MAE Department, Naval Postgraduate School, Monterey, CA, USA, 2018.

[3] M. Bualat, J. Barlow, T. Fong, C. Provencher, T. Smith, and A. Zuniga, "Astrobee: Developing a free-flying robot for the international space station," *AIAA Sp. 2015 Conf. Expo.*, pp. 1–10, 2015.

[4] NASA Ames Intelligent Robotics Group, "Astrobee Guest Science Guide," Moffet Field, CA, 2017.

[5] I. W. Park, T. Smith, H. Sanchez, S. W. Wong, P. Piacenza, and M. Ciocarlie, "Developing a 3-DOF compliant perching arm for a free-flying robot on the International Space Station," *IEEE/ASME Int. Conf. Adv. Intell. Mechatronics, AIM*, pp. 1135–1141, 2017, doi: 10.1109/AIM.2017.8014171.

[6] T. Rybus and K. Seweryn, "Planar air-bearing microgravity simulators : Review of applications, existing solutions, and design parameters," *Acta Astronaut.*, vol. 120, pp. 239–259, 2016, doi: 10.1016/j.actaastro.2015.12.018.

[7] V. Pletser, "Short duration microgravity experiments in physical and life sciences during parabolic flights: the first 30 ESA campaigns," *Acta Astronaut.*, vol. 55, pp. 829–854, 2004, doi: 10.1016/j.actaastro.2004.04.006.

[8] P. Von Kampen, U. Kaczmarczik, and H. J. Rath, "The new Drop Tower catapult system," *Acta Astronaut.*, vol. 59, pp. 278–283, 2006, doi: 10.1016/j.actaastro.2006.02.041.

[9] R. Zappulla, J. Virgili-Llop, C. Zagaris, H. Park, and M. Romano, "Dynamic air-bearing hardware-in-the-loop testbed to experimentally evaluate autonomous spacecraft proximity maneuvers," *J. Spacecr. Rockets*, vol. 54, no. 4, pp. 825–839, 2017, doi: 10.2514/1.A33769.

[10] NASA Ames Intelligent Robotics Group, "SPHERES/Astrobee Working Group Meeting." Mountain View, 2017.

[11] K. Nagaoka, R. Takano, T. Izumo, and K. Yoshida, "Ciliary Micro-Hopping Locomotion of an Asteroid Exploration Robot," *Proc. 11th Int. Symp. Artif. Intell. Robot. Autom. Sp.*, 2012.

[12] T. Yoshimitsu, A. Tomiki, K. Yoshikawa, and T. Kubota, "Operational results of

MINERVA-II twin rovers onboard Hayabusa2 asteroid explorer," in *International Astronautical Federation*, 2019, no. Part 1, p. 52276.

[13] A. R. Bradstreet, "Design, integration, and testing of an autonomous multi-body spacecraft simulator for low gravity hopping and grasping," M.S. thesis, MAE Department, Naval Postgraduate School, Monterey, CA, USA, 2017.

[14] J. L. Komma, "Mechatronics: The development, analysis, and ground-based demonastrations of robotic spacecraft hopping with a manipulator," M.S. thesis, MAE Department, Naval Postgraduate School, Monterey, CA, USA, 2018.

[15] S. T. Kwok Choon, J. Chitwood, C. Safbom, P. Leary, and M. Romano, "Astrobatics: A hopping-maneuver experiment for a spacecraft-manipulator system on board the international space Station," in *Proceedings of the International Astronautical Congress, IAC*, 2019, vol. 2019-Octob.

INITIAL DISTRIBUTION LIST

1. Defense Technical Information Center
   Ft. Belvoir, Virginia

2. Dudley Knox Library
   Naval Postgraduate School
   Monterey, California